Construction and Building Materials 308 (2021) 124995

Contents lists available at ScienceDirect

Construction and Building Materials

journal homepage: www.elsevier.com/locate/conbuildmat

Large-scale characterisation of cemented rock fill performance for exposure stability analysis

Bre-Anne Sainsbury [a,*], Saba Gharehdash [a], David Sainsbury [b]

[a] School of Engineering, Deakin University, Geelong, VIC 3216, Australia
[b] Geotechnica, Melbourne, VIC 3000, Australia

ARTICLE INFO

Keywords:
Cemented Rock Fill (CRF)
Large-scale laboratory testing
Direct shear testing
Three-point bending tensile testing
UCS

ABSTRACT

A novel large-scale geomechanical laboratory testing program is developed to provide full characterization of the strength and deformational response of cemented rockfill (CRF) material for use in exposure stability analyses. Uniaxial compressive strength (UCS), direct shear, and three-point bending tensile tests are performed on large-scale samples that require the use of novel processes and laboratory equipment. For the first time, the shear properties of large-scale CRF samples have been investigated using direct shear tests under constant normal stiffness (CNS) boundary conditions. Large-scale three-point bending tests are also conducted to obtain true tensile strengths without having to infer them from UCS test results. For up to 28 days curing time, the effects of particle size distribution and binder quantity are experimentally examined for each compression, tension, and shear failure mode through a study of the full stress–strain response. In order to obtain accurate laboratory results, findings are compared against published large-scale tests from various mine sites. The results show that the large-scale samples completed herein provide a reliable UCS estimate with standard deviations of less than one. It is also found that the direct shear responses are substantially larger for simulated CRF: Sidewall contacts than CRF: CRF contacts, and tensile strength responses are higher than previously estimated at 10% of the UCS strength. The effect of particle size distribution on the geomechanical response of the CRF material is highlighted through the large-scale sample testing. The findings of this research study provide increased technical understanding for the development of CRF structures in underground mines that are cost-effective, safe, and durable. Additionally, this research study establishes a practical testing methodology that overcomes the challenges that occur in collecting quantitative geomechanical data from large-scale CRF samples for design purposes.

1. Introduction

Ground instability is a major concern for narrow, irregular shaped ore bodies and orebodies in weak or highly stress environments. In each of these cases, a stoping mining method is usually employed to limit ground displacement and waste rock generation. The stoping mining method creates a continuous sequence of underground excavations (stopes) - the stability of which becomes critical for subsequent mining activities. Filling the stopes with the generated waste rock material reduces the environmental impact of mining through a reduction in surface waste-dump requirements. For many stoping operations, a stabilized waste material is commonly used to maximize extraction ratios [1]. It is also routinely used for the provision of access/re-entry requirements, passive hangingwall support, and the retainment of loose fill material [2-8]. A typical mining, waste backfill and exposure sequence in stoping operations is presented in Fig. 1.

The most common methods for increasing the strength of the stabilized waste fill material (e.g., backfill) includes stabilization with additives such as lime, Portland cement [9], waste/recycled materials (e.g., shredded tire) [10], and nanoscale/fibre stabilizers [11-15]. Among the stabilization methods, the inclusion of cement is the most widely used technique for stoping mines [1,9,16], and has been a ground improvement technique in geotechnical engineering for many years [15]. Even a small cement addition can make noticeable improvements in the stability of waste rock aggregate behaviour [1,17].

Cemented rockfill (CRF) is a stabilized fill material that is made by crushing waste rock, building debris or other waste solid materials before bonding with cement and water [1,9,16]. In some cases, the material is screened for particle size first. Fill mining with CRF is a green mining technology that not only solves the waste of land resources

* Corresponding author.
E-mail address: breanne.sainsbury@deakin.edu.au (B.-A. Sainsbury).

https://doi.org/10.1016/j.conbuildmat.2021.124995
Received 28 February 2021; Received in revised form 11 September 2021; Accepted 18 September 2021
Available online 30 September 2021

caused by waste dumps on the surface, but also effectively reduces strata movement. As a result, it provides significant economic, environmental, and engineering safety benefits.

CRF is the most operationally flexible and cheapest stabilised backfilling material to implement when infrastructure requirements are considered at established stoping operations [18,19]. CRF is preferred at many operations over other backfill materials (e.g., cemented paste backfill and hydraulic fill) due to its higher strength [7,20-24], increased stiffness, fast curing rate and lower capital cost [21]. It is also easily implemented once operations have commenced and can be of benefit to increase the extraction ratio [1]. These benefits are delivered by CRF with no additional binder cost when compared to other stabilised backfill materials [1,25,26].

The primary goal of CRF design optimization is to decrease the cost of backfill materials in mines. Optimization of CRF performance includes the modification of the ratio of water, cement, and waste rock to establish a 'mix recipe' that provides an adequate strength for the lowest possible cement addition. Reducing the cement content by as little as 0.5% can save operations millions of dollars a year [1] - not to mention benefits of increased availability of mobile equipment (e.g., agitator, loader etc.), and better working conditions (e.g., decreased heat produced and decreased circulating cement dust). An efficient CRF mix can also provide significant benefits to a mine in relation to costs and exposure stability [9].

The geomechanical performance of backfill materials are frequently obtained using a combination of analytical methods [27,28], empirical designs [29,30], experimental [31-33], and numerical modelling [31,34,35]. Analytical and empirical approaches generally consider the backfill as a homogeneous material simplifying the property parameters to include only the UCS strength and static ground stresses [26]. As such, it is generally agreed that in-situ testing is the most accurate for characterising the geomechanical response of a material. The challenge with in-situ stress and modulus measurements is that they are difficult and expensive and only establish the current stress–strain state of the material. The entire stress–strain path must be determined from combined experimental and numerical modelling [35,36]. For these reasons, it is recommended that in-situ testing must be coupled with a laboratory investigation program and numerical modelling to predict the scale-dependant, ultimate and in-situ performance of the backfill material.

As such, the results from both laboratory investigations and routine quality control testing are essential in delivering an optimized CRF exposure strength [26,27]. The required CRF strength is a function of the geometry of the excavation, mining method, backfill sequence and possible failure mechanisms [27]. Failure mechanisms are determined by the strength of the CRF and by the means of exposure (vertical or horizontal) and the order in which the exposure occurs. Some CRF materials can be exposed up to five times (sides, top and bottom) during the mining sequence. In each of these exposures, the failure mechanism may evolve differently due to the variance in stress paths that will affect yielding/damage within the fill mass [26,37]. Historical failure mechanisms of placed CRF include caving, shearing, flexing, sliding, and rotation [27,38,39]. Sliding occurs due to the low frictional resistance between the backfill and the rock sidewall. Flexural failure occurs when the exposed fill mass fails in tension. Caving can occur because of stress arching or rotational collapse due to the low shearing resistance at the rock sidewall [40]. The exposure and typical in-situ failure modes are presented in Fig. 2.

To provide adequate strength while minimising costs, a thorough understanding of the mining geometry, exposure sequence and host rock characteristics is required. Previous CRF optimizations have been achieved through the consideration of the following rules-of-thumb: 1) vertical exposures require less CRF strength than horizontal exposures, 2) lenticular exposures require less CRF strength than square exposures, 3) longer CRF curing times prior to exposure require less early-age strength, 4) sub-vertical dipping stopes require increased CRF strength compared sub-horizontal stopes 5) softer rock masses with convergent sidewalls require increased CRF strength / stiffness to maintain stability [1].

Routine laboratory testing of a backfill material provides an improved understanding of the critical factors influencing the strength, deformation, and post-failure response under a controlled stress environment. Backfill strength and curing rates have been historically characterised by UCS testing [17,41], and in some cases large-scale specimens were used [17,35,41-43]. However, there is currently no unique testing procedure that can correctly reproduce all of the unique stress paths that CRF is subjected to in-situ in the laboratory. Many researchers have employed triaxial and UCS testing to explore certain features of CRF behaviour [8,17,36,44]. However, these stress conditions provide only an estimate of the resistance of the material to one-dimensional crushing. Of all the observed failure mechanisms of CRF in-situ, the occurrence of crushing is the most unlikely during horizontal (overhead) and/or vertical exposure in an extraction sequence [1,39]. Compression testing of CRF material is often used since the required equipment and methods are easily available, and the samples are straightforward to prepare. As such, the majority of existing literature focuses on exploring compressional responses of backfill material.

Depending on the size of the samples, several compressive strength test equipment and measurement methodologies have been employed for UCS testing of granular material [17,25,36]. However, as discussed previously, compression is not a likely failure mode for CRF material in-

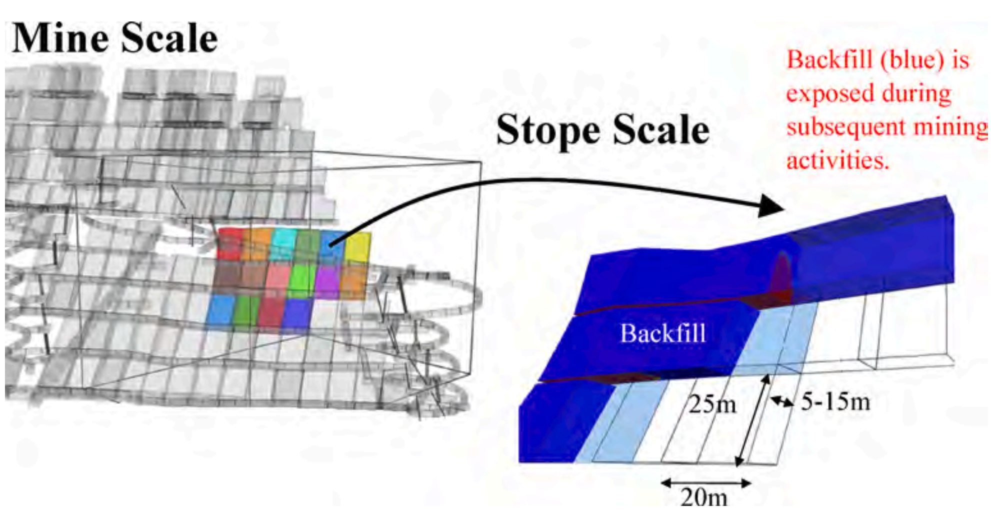

Fig. 1. Typical mining backfills and exposure geometry in underground stoping operations.

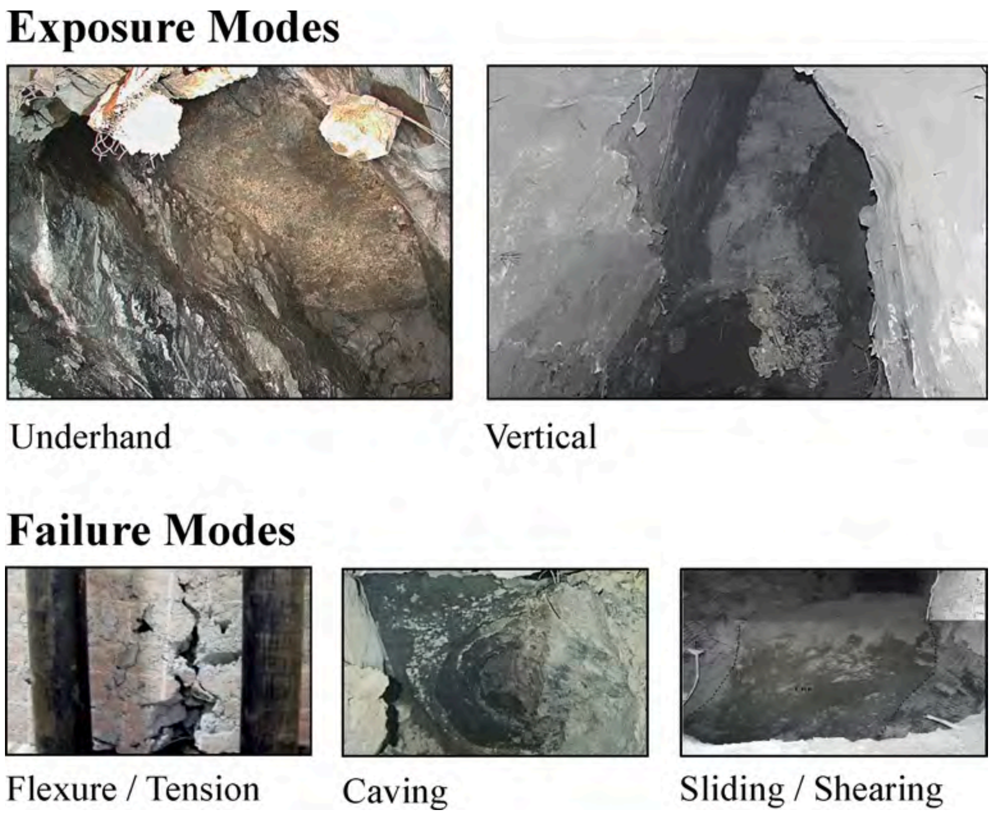

Fig. 2. Observed backfill exposure and failure modes in underground mines. Flexure presented after [40].

situ. This suggests that past research findings are insufficient to provide a thorough knowledge of CRF mechanical behaviour. Based on observed failure modes and numerical models, the shear and tensile strength of large granular materials are the most critical parameters for design of structures such as rock fill embankments, railroad sub-bases [45,46] and CRF [25]. However, due to the large-scale specimens required to characterise the in-situ response, the number of laboratory facilities equipped to test these materials are few. And, as such, to date, the shear and tensile behaviour of large-scale CRF samples have not been investigated by direct shear and three-point bending test methods.

In this research, cost-effective experimental design is documented for large-scale CRF material containing particle sizes up to 100 mm. Reliable experimental procedures are demonstrated for a range of stress paths that include compression, tension, and shear to obtaining qualitative and quantitative data. A total of 119 unconfined compressive strength (UCS) tests, 8 direct shear tests, and 4 three-point bending (3 PB) tests are conducted to obtain the large-scale performance of CRF in-situ. To date, direct shear and three-point bending tests have not been completed on CRF samples of such a scale. Furthermore, reliable data on the tensile and shear deformation behaviour of CRF and how it is impacted by aggregate gradation, and binder content are also presented that have not been previously considered.

2. CRF performance contributing factors

Contributing factors for the geomechanical performance of CRF have been previously studied and are summarized below to provide context for the current research that is presented herein.

2.1. Particle size distribution (PSD) and sample size

Large particles, either from crushed rock or mining debris, are frequently used in the development of CRF. Particle size has been previously shown [47,48] to have the most significant impact on CRF strength and stiffness since it controls the porosity/density of the mix [49,50]. For example, a mix that has a low fines content will have an increased porosity reducing the strength and stiffness since it is relying on the discrete point-to-point contacts of the granular assemblage (there is minimal surface area in contact). On the other hand, a mix that has increased fines will have a larger particle surface area, lower porosity, and result in a stronger and stiffer material. We note here that it is also likely to require more cement to bind the particles together.

Usual mine waste has variable geology and has a relatively large maximum particle size (~500 mm) based on drill and blast practices [1,6]. This poses a challenge for testing, both in the size of the sample required to achieve a Representative Element Volume (REV) and because large particles give unrepresentative interactions at the limited laboratory scale. Examples of waste particle size variation in operations that are used for the development of CRF are presented in Fig. 3.

The large particle size implies that typical sample sizes cannot be used to reliably assess the laboratory strength of CRF. Small diameter samples may result in spurious outcomes owing to large particles dominating the strength response of a sample or impeding the flow/fracture of the material. As such, different experimental programmes have been established by researchers to investigate the effect of sample size on UCS.

At the Cosmos Nickel Mine large samples were prepared and tested (500 mm × 1000 mm - diameter × length), and were compared to the response of 150 mm, 240 mm, 300 mm, and 400 mm diameter samples. It was found that as the sample size increased the strength decreased [16]. In order to produce accurate geomechanical property data, it is clear that specific conditions for the sample size must be achieved. This is sometimes problematic since the particle size and sample mould size cannot be considered separately [51]. Removing oversized aggregate (larger than 1/3 of the diameter of cylindrical mould) significantly modifies the mix design and may result in increasing the cement-aggregate ratio [52] and increasing the apparent strength [53]. It has been shown that through sieving out oversize particles, the increase in

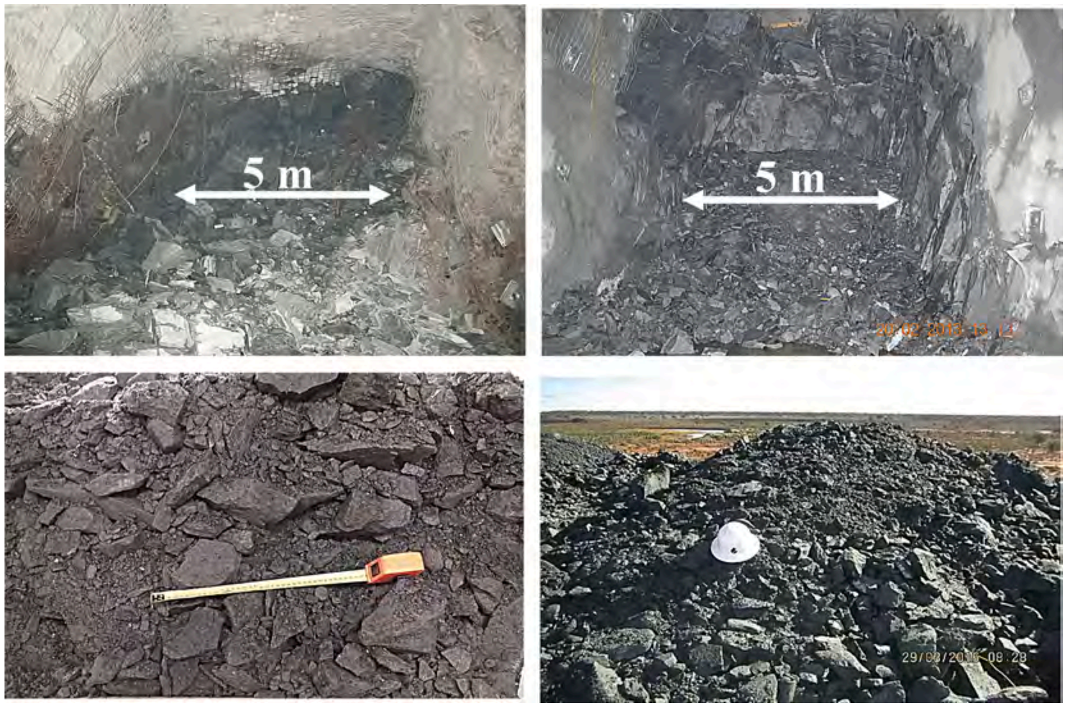

Fig. 3. Typical waste particle size variation at mine sites used in CRF development.

sample strength is directly proportional to the amount of large aggregate removed [52]. Marachi [54] found that through reducing particle size distribution parallel to the original sample size, accurate laboratory results can be achieved on a smaller scale. However, this hypothesis may be too simple since scale effects also alter behavioural characteristics [55]. Previous research studies [16] found that a sample diameter size of 400 mm provides the most reliable design basis in the laboratory for mine-based particulate matter. However, in general, the diameter of the test specimen should be (a) as large as possible and (b) at least five times the average particle size [56,57]. The ideal grading for a CRF in-situ has been previously described by Stone [48].

2.2. Particle shape

CRF materials are produced from blasting the rock and resulting particles are usually angular or sub-angular in shape [1,6]. The angularity of the waste rock particles can significantly influence the material response; not only through the consideration of porosity, but the effectiveness of the point-to-point contacts/bonds that the cement grout is able to achieve [1,6]. In general, an increased number of point-to-point contacts will increase the stiffness/strength of the mix, and an increased surface area associated with the point-to-point contacts will increase the stiffness/strength of the mix. If the particle shape characteristics of the waste rock used for the development of a CRF mix differ significantly across a site, it is recommended to blend the waste in a stockpile and/or optimize the recipe for each waste rock separately. In either option, rigorous quality assurance and quality control [26] during the waste rock selection/stockpiling and mixing is required to ensure the desired strength of the CRF is achieved.

2.3. Particle intact strength and micro-flaws

Historically, the strength of the waste rock material used for CRF has not been considered significant in the overall design performance. This assumption is only valid, so long as the waste rock is stronger than the grout mix used, and it doesn't include significant micro-defects flaws/ anisotropy that may cause intact block failure and/or a preferred orientation of weakness. It is also assumed that the waste rock does not include clay material that will degrade over time. Laboratory testing [58] shows how the introduction of a relatively weak waste material produces more fines during the mixing process resulting in a stronger mix (due to a higher bulk density and lower void ratio). As a result of this, it is critical to identify and characterize the waste rock strength as part of the laboratory testing program [26]. As a general guideline, Stone [59] suggests that aggregates for CRF have a UCS value of 70 MPa or higher.

2.4. Moisture content

The moisture content of waste rock can be highly variable; both underground and during the transportation and storing in partially sealed containers in the laboratory. To minimize the impacts of a variable moisture content, waste rock is must to be blended prior to batching. The moisture content in sub-samples within the laboratory should be determined prior to batching and mixing and considered during the development of the batch-mix [1,59].

2.5. Water/cement ratio

The water-to-cement ratio has an impact not only on CRF strength, but also on the workability of the backfill material during placement. Traditional concrete has a water-to-cement ratio of 0.4 to 0.5, whereas most cemented rockfills have a ratio from 0.7 to 1.2 [1]. Generally, the lower the water-to-cement ratio, the higher the strength of the fill; however, at lower water contents, the resultant backfill can appear to be very dry and segregates easily. It can also be harder to place in stopes that are sub-vertical [1,59].

CRF mixes with a water: cement ratio of 0.8 are recommended for the design specification with an additional proportion of water able to be added during placement (up to a water: cement ratio of 1.0) to achieve the desired flow characteristics. Additional water that can be added in-situ during mixing/placement and is usually defined in litres per loader bucket of mixed CRF [1,6,59].

2.6. Water quality, cement content, and curing time

Since many of the strength-dependent factors of CRF are unable to be modified (e.g., quality of raw materials, particle shape and size) the cement content is the most direct way to vary the strength performance. It has also the highest cost and therefore optimization of its inclusion is necessary.

The effect of water salinity on the strength development of CRF is well documented [58]. Increased total dissolved solids [58] provides a negative impact on CRF strength development. As a result of this, it is critical to use representative mine water to mix the laboratory samples. However, when mine water is used, it is possible that chemical reactions may result in corrosion/oxidation and decrease the strength of the mix over time. Pierce [60] has previously characterized the decrease in strength with curing time in humid-curing conditions of paste fill samples at the Golden Giant Mine due to oxidation. Testing with mine water at 7, 14, 28 and + 28 days is recommended to determine the long-term strength characteristics [7,9,60]. Cemented backfill is typically designed to achieve its maximum compressive strength after at least 28 days curing [61]. It has previously been shown by researchers that the strength of CRF remains unchanged, beyond approximately 28 days [7,9,17]. It is also likely that exposure of the material in-situ will also occur around this timeframe.

3. Laboratory testing program

A robust and comprehensive laboratory testing program of CRF is outlined herein that address each of the contributing factors outlined in Section 2. The results provide geomechanical characterisation of the expected CRF performance (strength and deformation) that can be used to assess large-scale exposure stability. CRF performance has been characterized through three distinct laboratory stress paths that include UCS, direct shear and Three-Point Bending (3 PB) tensile tests. A summary of the CRF waste rock material, mix design and laboratory tests performed are detailed in Sections 3 to 6.

3.1. Materials

3.1.1. Waste rock aggregate

Waste rock aggregate in this research study were derived from a number of mine sites in Australia. The UCS of the intact rock particles ranged between 50 and 100 MPa. The variability of the CRF material has been limited by the removal of clay components and by screening out particles larger than 400 mm in all cases [1].

3.1.2. Binders

Binders are selected based on the strength and durability requirements of each mining operation. It is generally made from a combination of cement clinker and calcium sulphate (usually gypsum). Because of its availability and adaptability, ordinary Portland cement (OPC) is the most commonly utilised binder agent at mines. The physical properties of Portland cement are provided in Table 1.

OPC has been used in the development of all CRF samples prepared, tested, and presented herein.

3.1.3. Water

Water functions as a lubricant, improving the workability of CRF and creates the essential ingredient for cement hydration. Impurities (dissolved or suspended) in the mixing water can lower the strength of any form of minefill [62,63]. Herein, for CRF mixing, the relevant mine water has been used for the development of all samples and strengths tested at different curing ages to determine the impact of corrosion/oxidation.

3.2. Mix design

CRF samples for testing can be prepared underground (Fig. 4a) or in a laboratory (Fig. 4b) [1,6]. Sample preparation methods can have a significant effect on test results. In each of these cases, there are several issues that need to be considered when interpreting the test results.

If the CRF samples are mixed underground in 'mine conditions', they are likely to develop cracks and fractures when being transported to the testing facility. As a result of this induced damage, the strengths measured in the laboratory may under-estimate the true in-situ response. If the CRF is mixed and cured in a laboratory, it will not be at typical 'mine conditions' that usually include elevated temperature and humidity. However, limited damage to the samples will be induced during a transportation event. To ensure the most accurate results, it is recommended that mixing be undertaken within the laboratory. Samples can be batched and placed into a curing chamber. Laboratory mixing also provides the opportunity for an accurate particle size distribution to be conducted and ensure consistency between sample responses and testing procedures. Relationships between laboratory mixed and mine-conditions may be derived.

In order to obtain accurate test results for the current research, a consistent mixing method was used for all specimens. All samples were developed in general accordance with ASTM [64]. The required weight of aggregate and cement (by weight of dry rock aggregate) were mixed in a drum concrete mixer with a maximum capacity of 0.5 m^3. Based on estimates of in-situ CRF densities a homogeneous starting testing density of 2000 kg/m^3 was defined. Mixing was performed at a rate of 12 revolutions per minute, with the tilt of the mixing bucket being adjusted numerous times to ensure optimum blending. To create the appropriate CRF mixture, water was then added to the cement and aggregate and the material was homogenised for ~ 10 min. The homogenous CRF mixture was then placed into both cylindrical and cubical moulds, depending on the test procedures to be undertaken. The specimens were cured at a temperature of 25° ± 2 °C and relative humidity above 90% for 7, 14, 21, and 28 days prior to testing.

3.3. Particle size distribution (PSD) analysis

The difficulties in laboratory tests on cemented rockfill materials usually lay in determining aggregate particle size and selecting a suitable sample size. The American Society for Testing and Materials (ASTM) [56] proposed that the minimum diameter of a cylindrical specimen is three times larger than the aggregate maximum particle size to eliminate the size effect. Wu et al. [57] suggested that the specimen diameter is at least five times larger than the maximum particle size. To determine the particle size distribution of the CRF samples presented herein, a 200 kg material sample of each mine waste was sieved into various size intervals of 12.5, 25, 50, 75 and 100 mm. The resulting particle size distribution (PSD) of each mine waste is provided in Fig. 5.

Talbot and Richart [47] have previously developed an equation for the optimisation of waste rock grading for CRF [65] that is presented in Equation (1).

Table 1
Physical properties of Portland cement [15].

Blaine (cm^2/g)	Expansion (autoclave) (%)	Specific gravity	Compressive strength (kg/cm^2)		
			3 days	7 days	28 days
5808	0.05	3.1	185	295	397

Fig. 4. a) Sample preparation underground, b) batch mixing in a laboratory, c) samples prior to capping, d) sample capping.

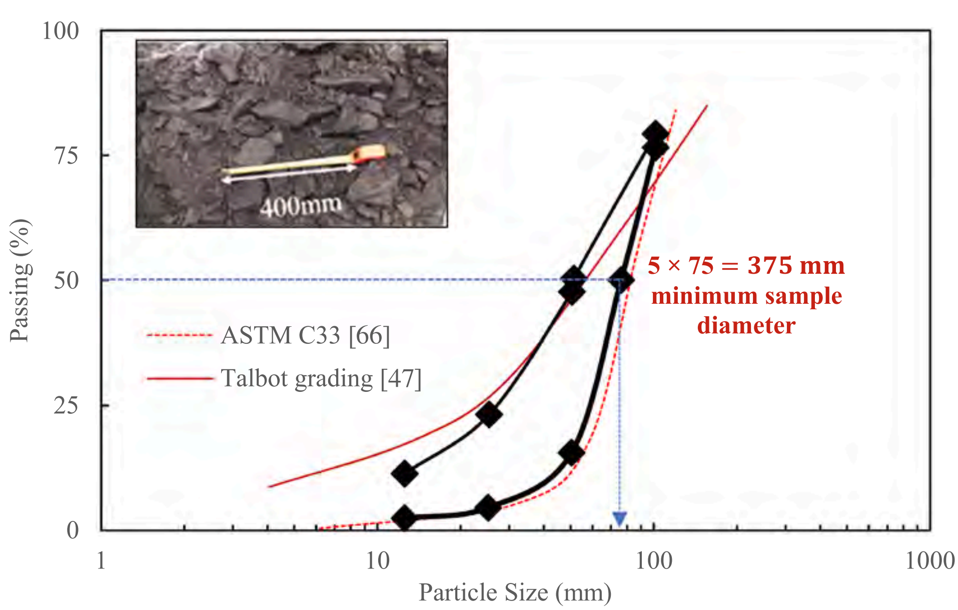

Fig. 5. Characteristic particle size distribution (PSD) of waste tested and indication of minimum sample size diameter.

$$P(d) = 100\left(\frac{d}{d_{max}}\right)^{n} \tag{1}$$

where P is the percentage of aggregate which passing the sieve size d by weight, d_{max} is the maximum aggregate size, and n is an experimentally defined constant. Swan [65] established an optimal n value for cemented backfill and Fig. 5 displays the aggregate size gradation that satisfies the recommended technique [66] for estimating the particle distribution of cemented backfills (solid red line).

The PSD results reveals that the waste aggregate used transitions from a fine to coarse size more quickly than the optimal theory of CRF aggregates suggests [65]. Given that rock aggregate particles with a diameter of less than 10 mm are considered fine aggregate, the experimental rock aggregate used in this study is composed of approximately

≥ 85% coarse and ≤ 15% fine aggregate by weight. The maximum average particle size (d_{50}) is observed to be ~ 75 mm. To ensure scale effects are minimised, a sample width of five times the average particle size is required [57]. e.g. ≥ 375 mm diameter.

4. Unconfined compressive strength (UCS) testing

The unconfined compressive strength (UCS) test is the most common method for determining backfill strength, and it is often utilised for quality assurance and quality control at mining operations. UCS testing provides an estimate of the CRFs material to withstand crushing. In-situ, crushing may be caused by imposed loads (driving over it) and/or sidewall convergence. Although crushing is the most unlikely failure mechanism underground [1,6], UCS tests are the easiest to conduct in the laboratory and shear and tensile strengths can be inferred from their results.

4.1. Sample preparation

Cylindrical samples with a height to diameter ratio of 2.0 were prepared in general accordance with ISRM standards [67]. A sample size of 406 mm diameter × 812 mm height was chosen for the UCS testing. This size is greater than the required 375 mm diameter determined from the PSD analysis (Section 3.3). A cement cap was applied at both ends of the sample to provide a smooth testing surface and ensure homogeneous distribution of the load during testing [68] (Fig. 4c, d). Through this geometry and capping, the samples are able to fulfil test criteria associated with the statistical validity of test results, integrity, parallelism, and perpendicularity.

Sub-sampling of the bulk waste material can result in samples being created with a significant variance in PSD. In the case presented in Fig. 6 each of the samples were generated from the same mine site, have the same cement content (6% by weight) and dimensions (400 mm × 800 mm). However, the UCS strengths generated range from 0.2 MPa (largest average particle size) up to 3.0 MPa (smallest average particle size). These findings are consistent with experimental results provided in previous investigations [16,69]. As such it was critical to ensure the PSD was clearly identified for each sample and considered in the results analysis.

Samples have been tested at curing times of 7, 14 and 28 Days and cement contents ranging from 2% to 8% (by weight).

4.2. Testing apparatus

A 600-kip, manual-hydraulic driven, stiff-frame test machine was used to test the UCS cylinders. An Amsler compression load frame with an axial load capacity of up to ± 5000kN was used to apply the static load on the large-scale samples. The tests were carried out at a constant rate of deformation of 2 mm/min (computer controlled). This loading rate was determined based on a series of tests that were conducted on 6% CRF samples that were been cured for 14-days. The effect of loading rate on the CRF sample failure is illustrated in Fig. 7. With increased loading rates, the stress–strain curve presents different failure mechanisms. At a high loading rate, the sample appears to have a higher peak strength. Higher loading rates cause a dynamic 'shock' response and post-peak brittle behaviour. This phenomenon is well documented through numerical analysis [70]. A loading rate of 2 mm/minute was applied to all UCS samples for the current study samples since localisation and post-peak brittleness is not observed at this value.

An electronic acquisition system was used to automatically record the axial loads and deformations. The axial strain on the samples was measured using two linear variable differential transformers (LVDT) which were attached to the base plate. To ensure minimal damage to the samples they were placed within the loading frame prior to the formwork being removed (Fig. 8).

4.3. Test results

A relationship between cement content (cc%), UCS and Deformation Modulus is derived for the 28 days cured results (Fig. 9 and Fig. 10 respectively). The UCS and modulus values were determined according to the ISRM methodology [71]. A R^2 fit of 80% and 70% is achieved for each respectively.

These results show that a higher cement content leads to a rapid rate of strength and stiffness gain during the early stages of curing (up to 28 days). Due to hydration, the CRF sample strength rises in proportion to

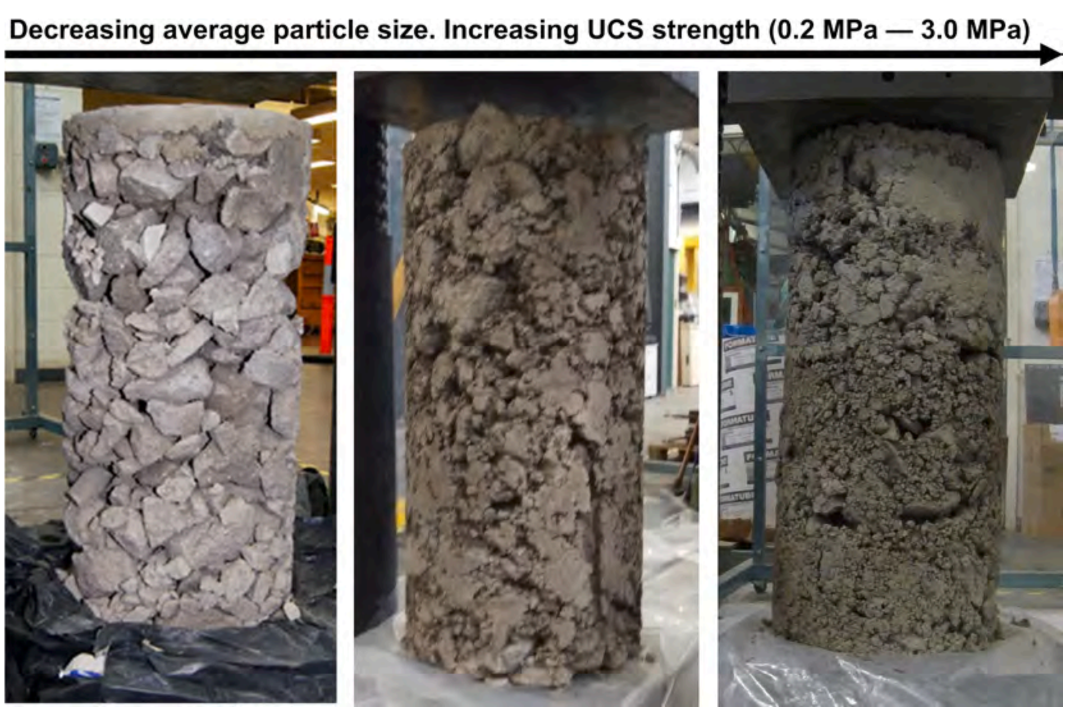

Fig. 6. Decreasing average particle size versus UCS.

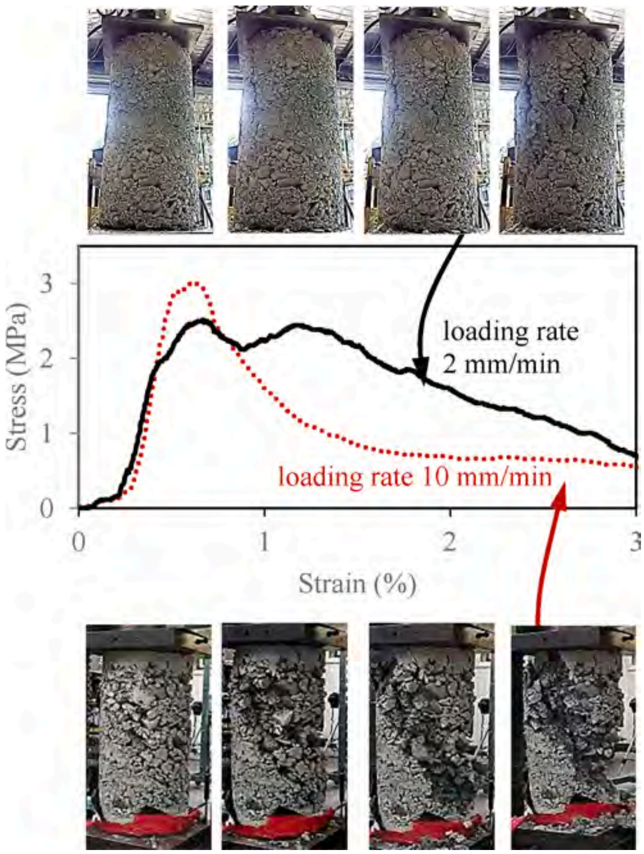

Fig. 7. Consideration of UCS loading rate for large-scale CRF samples.

the quantity of cement utilised. e.g., 8% cement content samples provide a faster rate of strength increase than 3% samples for up to 28 days curing. It is also observed that with increased curing time, the CRF samples present less ductility or plastic behaviour. Selected characteristic stress–strain curves for each of the cement contents tested are provided in Fig. 11.

During the early stages of loading, cracking of the cement bonds was clearly audible. With increased load the sample entered the brittle/ductile transition phase where the rockfill particles were observed to rotate and interlock. In the post-peak phase, the interlocking particles could be observed to dislocate in a controlled manner. The sample maintained approximately 50% of its peak UCS load after 1% of post-peak straining in the 3%-7% cement samples. The 8% CRF sample failed in a violent brittle manner. In fact, the full stress–strain curves in Fig. 11 show that as cement content increases, so does the post-peak brittleness, transitioning from characteristically ductile responses at 3% cement to perfectly brittle at 8% cement content. This is a significant new finding that can be used directly in strain-softening numerical models for exposure stability analysis.

4.3.1. Validity and repeatability of the experiments

To examine the validity and repeatability of the current large-scale UCS laboratory test results, the strength variation of 3% (cement by weight) samples based on sample size, along with standard deviation were compared to equivalent published data from different mine sites. The results are presented in Fig. 12.

The findings show that 400 mm diameter samples provide less fluctuation in UCS strength (Fig. 12a, b). In addition, except for the 400 mm diameters samples, the standard deviation increases with curing time for all sample diameters. This reduction in variation for the 400 mm samples suggests the larger sample size provides better representation of the CRF mix. E.g., the samples are large enough in relation to the average particle size [56]. With increasing sample size, CRF samples show a general decline in strength (see Fig. 12a) and therefore provide a more accurate testing results for the in-situ CRF placement [9,16,74].

Specimens' tests from published mix designs [16] and the current results were also compared (Fig. 12c) to determine the validity of the current results. As can be seen, despite the variation in mixture design from different mine sites, the 400 mm and 500 mm samples show less UCS variation than the smaller samples. As a direct result of these analyses, the current test findings are considered accurate, valid, and repeatable since the average error between the current study and published results from sample sizes of 400 mm and 500 mm [16,69] was less than 5%.

4.3.2. Effect of sub-sampling

The variation in UCS and modulus responses from specimens sub-sampled from two-tons of waste are presented in Fig. 13a, b. In each of the cases the average particle size of each specimen was recorded. For fixed 400 mm × 800 mm samples, and a variation in cement content from 3% to 8%, it can be observed that as the average particle size increases, the variation in the UCS and modulus decreases – regardless of the cement content. This suggests that the average particle size of the waste material may have more impact on the strength of the sample than the cement content when the d_{50} is above 75 mm. In-situ, this can suggest that ungraded CRF material placed in a stope may be less strong than expected but have a more consistent strength.

Fig. 13d shows a plot of modulus vs UCS for CRF samples from the Cannon, Stillwater, and CHUG Mines [9,72] compared to the current test results. Despite the inconsistent sample preparation processes and

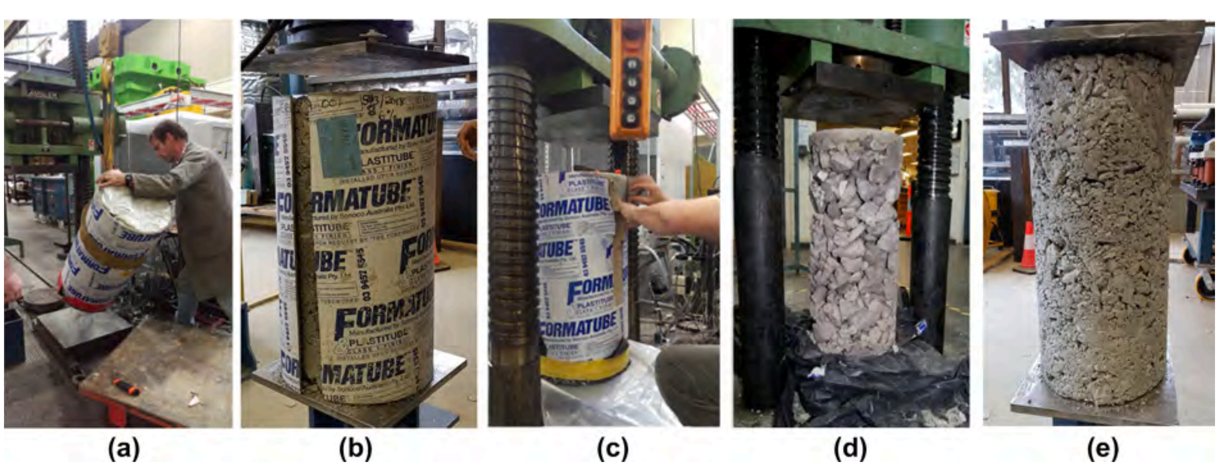

Fig. 8. a) Sample seating, b) & c) mold removal d) test setup e) loading.

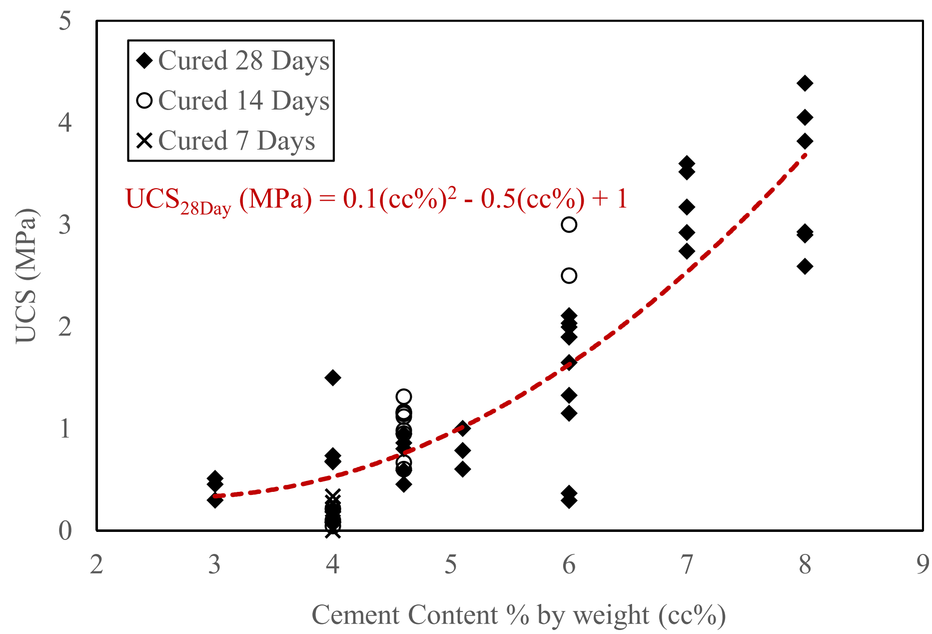

Fig. 9. UCS versus cement content and curing time.

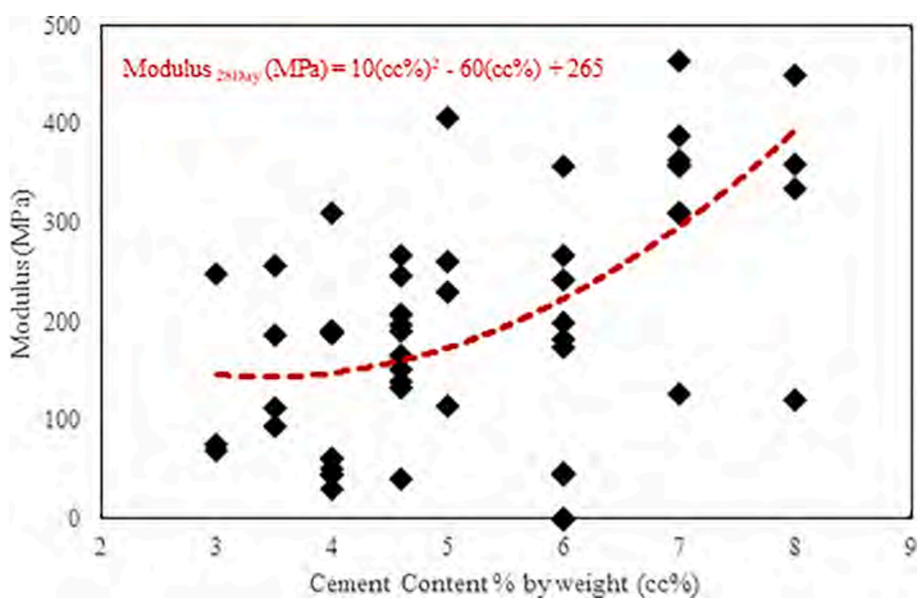

Fig. 10. Modulus versus cement content and curing time.

testing methodologies between sites and samples, the current study is consistent with other published findings. UCS experiments for large diameter cylinders, in-situ testing, instrumentation investigations, and numerical back-analysis of observed displacements were all used to derive these elastic modulus values presented in Fig. 13d. It can be seen from this chart that, the elastic modulus of a CRF sample reduces as the sample size rises, demonstrating that sample size and particle size have an impact on the modulus. In addition, there is a clear relationship between elastic modulus and UCS.

The influence of the curing period, as well as the size and particle distribution on the UCS of CRF samples from reference [17] and the current study is shown in Fig. 13c. The experimental results reveal that, regardless of the particle gradation, the UCS of CRF samples increases with increased curing time. Indeed, a longer curing period results in more cement hydration products, which contributes to a better hydration-bonded aggregate structure. However, it is shown that the rate of strength development decreases as curing time increases. In reality, the in-situ CRF should continue to increase in strength over time since most underground mines provide ideal curing conditions with the humidity rarely falling below 80% or the temperature falling below freezing [75]. However, most exposures occur within weeks to months of placement [1].

The time-dependent variations in the UCS are also seen to be a function of the particle size, as seen in Fig. 13c. The CRF sample with the largest grain size variability (e.g., smallest average particle size) provides higher UCS values than those with a lower particle size dispersion (e.g., higher average particle size). This can be attributed to the impact of the larger particle on the packing density of CRF mixes. A higher packing density results in a reduced void ratio in the CRF, which optimizes the CRF strength. The density of the samples can be influenced by

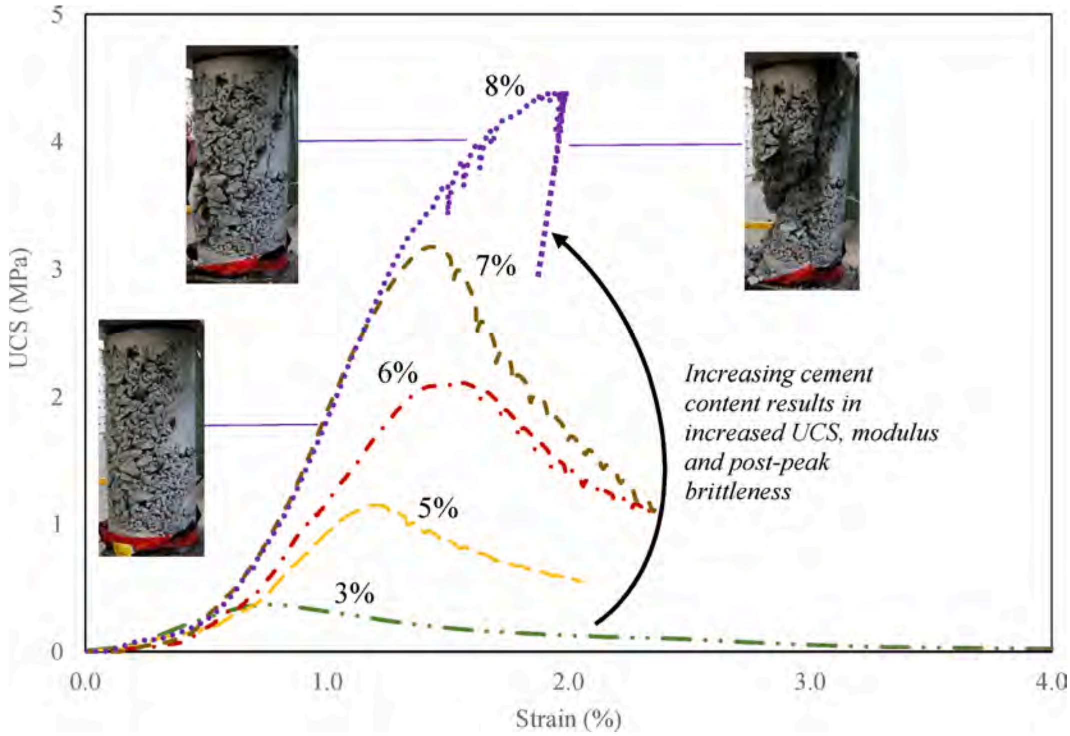

Fig. 11. UCS stress-strain curve, for 3%, 5%, 6%, 7% and 8% cement samples with 28-day curing.

a variety of parameters, including the fines concentration and the compaction obtained during casting/placement. The inclusion of fine grain material (e.g., less than 10 mm) component also affects the strength of the CRF samples as highlighted in Fig. 13. This implies that the proportions of aggregates and fine grain (soil) components in CRF mixes could be adjusted to increase compressive strength. This can be achieved through the drill and blast practices and/or screening the waste material prior to placement.

4.3.3. *Effect of curing time*

The impact of curing time and cement content has been considered on the UCS strength in Fig. 14a. Here the results for various curing times (±28 days) are presented. The maximum, median and minimum values are considered. These UCS test findings show that the strength of CRF increases with time, but the rate of strength development slows down as the curing time increases. Based on the laboratory results, as cement content increases so does the maximum, median and minimum values of the UCS measured. It is clear that curing ± 28 Days increases the minimum, median and maximum UCS values of the sample. This is observed to be more pronounced as the cement content increases.

The UCS of 153 mm × 305 mm CRF samples from the TRJV mine [18] that were cured for 5,927 days, and 708 days (more than 2 years and 16 years) were compared to the results of the current UCS tests, as well as the results of tests conducted at another mine after 7 and 28 days of curing [9,73]. The results in Fig. 14b reveal that all of the CRF samples have a similar trend in terms of time-dependent strength gain i.e., a fast increase in the UCS until 28 days, followed by a more gradual increase. The rate of strength increase is faster at earlier ages, but it slows down as time passes [73]. According to Seymour et al. [73], the UCS strength of CRF samples under controlled curing conditions increase over time in the same way that concrete does.

5. Direct shear testing

Large-scale direct shear testing has been previously completed on paste-fill samples to understand the internal and sidewall shear interactions [76,77]. Through this research study, the shear interactions between the CRF and rock sidewall and primary and secondary CRF stope interactions were considered through direct shear testing which is considered to be an appropriate method for this failure mode [25]. The constraints of the in-situ rock mass and fill material are easily represented through the shear box and a constant normal stiffness boundary condition [78]. Direct shear testing has been shown to provide an accurate estimate of the behaviour of CRF when subjected to shear strain [25,78].

5.1. *Sample preparation*

Two different direct shear test sample preparations have been completed that include CRF on CRF (CRF: CRF) and CRF on cured concrete (CRF: Sidewall) to represent the in-situ and sidewall contact interface [79]. Direct shear test samples have been prepared in moulds to provide a tight fit in the shear box. Moulds have been prepared with dimensions of 200 mm × 300 mm × 137 mm which have a diameter-to-length ratio of 0.67 which fulfils the required sample size for the maximum aggregate size [75]. In each of the cases, the direct shear samples were prepared with a thin mortar base and cap to ensure solid contact with the shear box, minimising point loading on the sample during shearing (Fig. 15a). They were cured in dry, indoor conditions to simulate in-situ conditions, which includes dry particle bonds due to air exposure [80,81]. After curing, samples were removed from the moulds and placed into the shear box. Direct shear samples have been tested after 28 days curing with 6% cement content. An example of a cured sample being prepared for testing is provided in Fig. 15.

5.2. *Testing apparatus*

Different loading conditions can be applied to a sample during direct shear testing. The sample can be subjected to constant normal stiffness (CNS) or constant normal load (CNL) boundary conditions. Shrivastava and Rao [85] and Poturovic et al. [86] designed a large-scale direct shear test apparatus employing a hydraulic servo-valve to replicate CNS

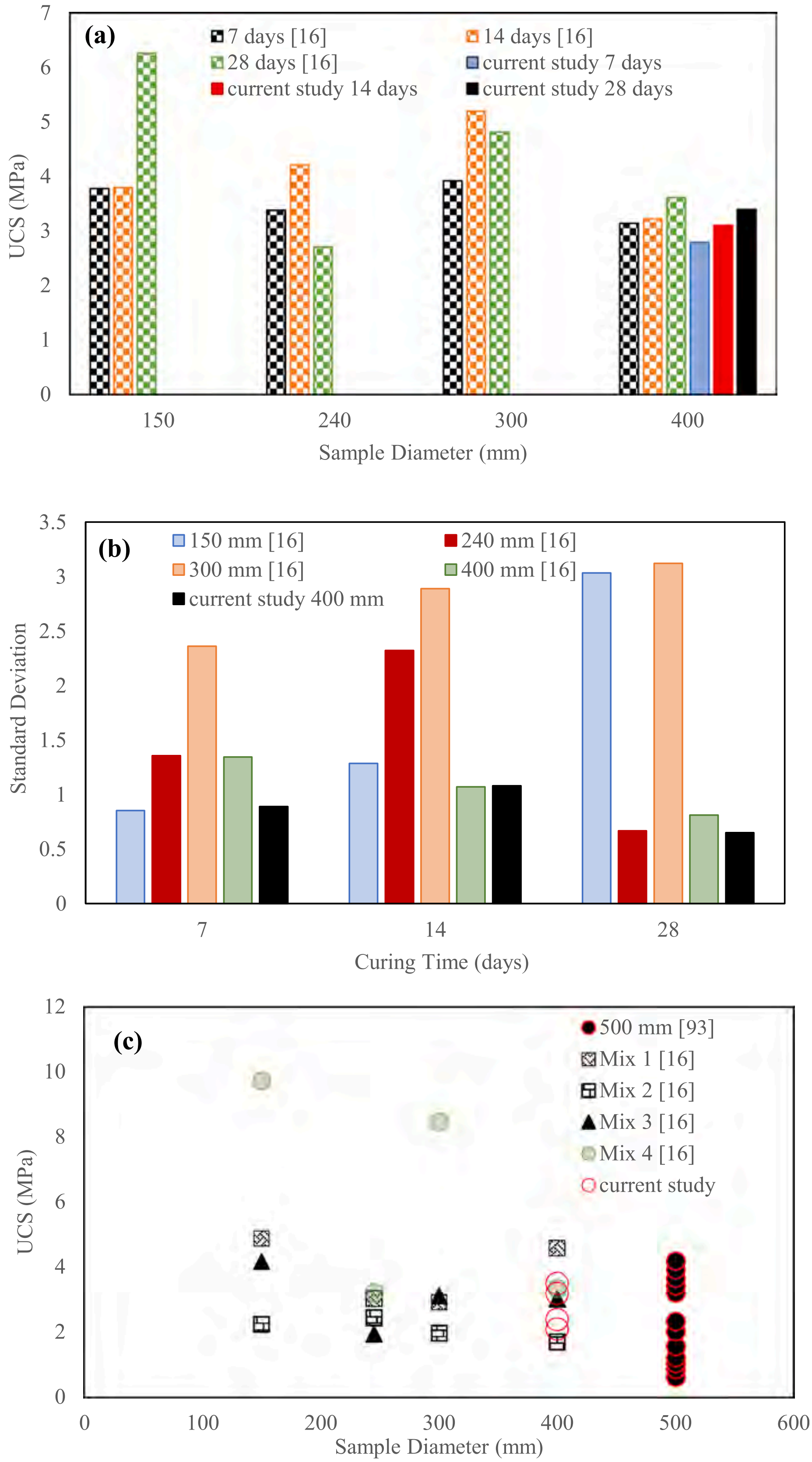

Fig. 12. (a) Average UCS versus sample sizes and curing time, b) UCS standard deviation for sample size and curing time, and c) comparison between current research study UCS and Cosmos Nickel Samples of 3% cement by volume at 28 curing days.

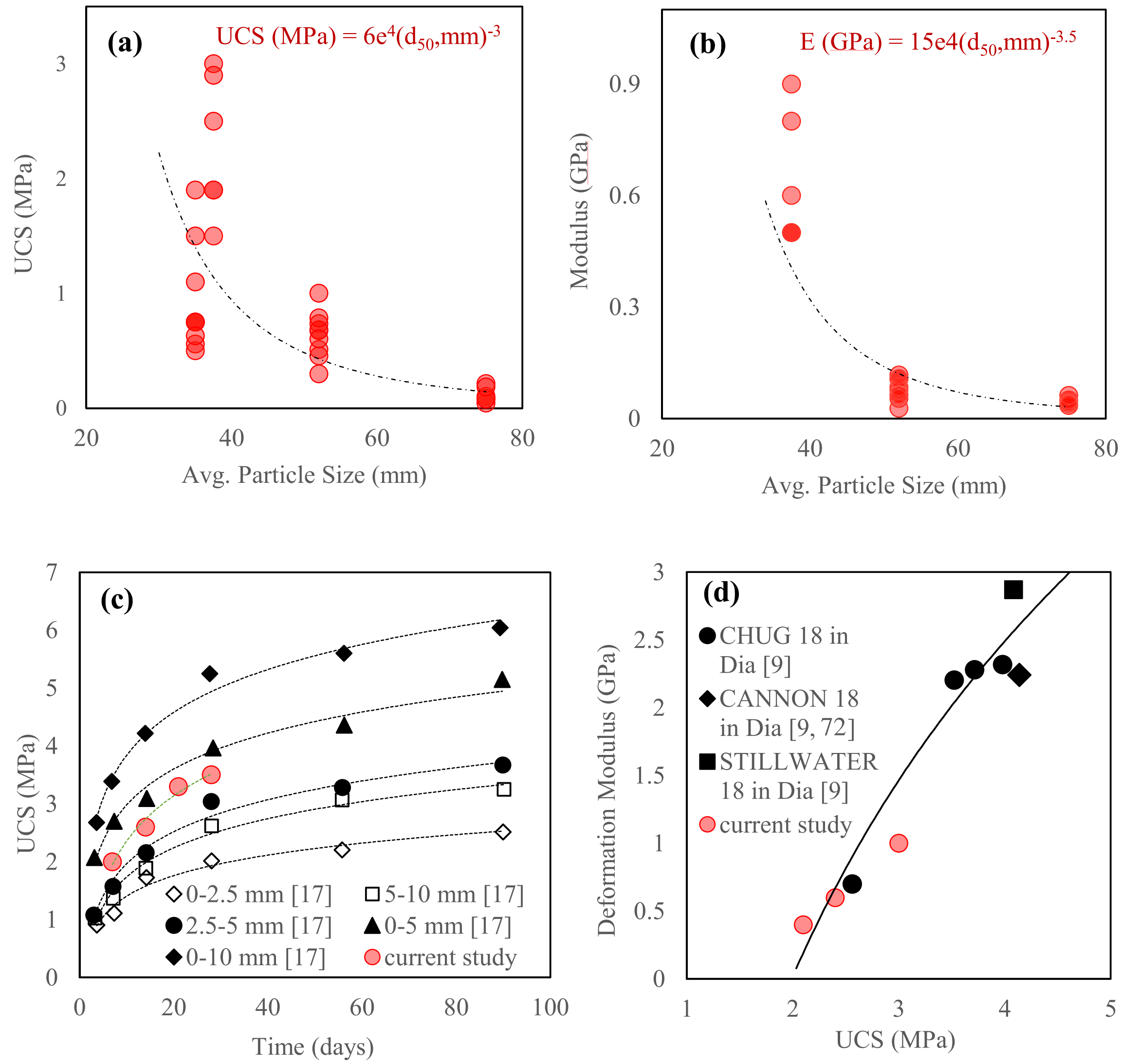

Fig. 13. a) UCS versus average particle size, current study b) deformation modulus versus average particle size, current study c) UCS versus average particle size, current & historical studies compared d) deformation modulus versus average particle size, current & historical studies compared [8,72]

boundary conditions. Thiel and Zabuski [87] conducted direct shear experiments in the field to determine the shear strength of Carpathian flysch. The shear tests were conducted using jacks under constant normal load (CNL) conditions. Afridi et al. [88] performed laboratory direct shear testing on intact Salem Limestone samples with a visible plane of weakness, and concrete-rock interfaces. The shear tests were carried out under CNL conditions, with normal stress applied to the sample ranging from 4 to 14 MPa [89]. Based on these historical results, it is reasonable to infer that there is no one laboratory approach that is ideally suited for examining the behaviour of CRF. It is agreed that direct shear testing, like all testing, is better conducted in-situ, however, preparing sufficient samples and conditions can be difficult and expensive. As such, the choice of testing apparatus becomes one of availability. According to research [78], boundary conditions with constant normal load (CNL) and constant normal stiffness (CNS) can significantly affect the interpreted shear properties of discontinuities. A sheared CRF will normally dilate as a result of the rock blocks rotating or sliding on joints. Depending on the circumstances, the surrounding rock mass may or may not resist this dilation. Testing under constant normal load (CNL) circumstances would be suitable if there is no resistance to dilation. However, this situation may apply to rock slopes that collapse. In many circumstances, the dilating rock compresses the neighbouring rock mass, which might be considered as a spring. The normal stress level rises as the amount of dilatation increases. As such, testing under constant normal stiffness (CNS) settings may be more appropriate in this in-situ scenario [78] and have been applied herein to determine the shear strength of CRF.

A shear apparatus capable of shearing rock mass samples under CNS or CNL conditions, has been used in this study [82–84]. Hydraulic actuators are used in the direct shear apparatus to apply normal and shear stresses. The load cells coupled to the actuator ram had a static capacity of up to 250 kN and an accuracy of 0.5 kN. For testing with very low initial normal stresses (e.g., 100 kPa), the vertical actuator of the load cell was replaced with a 50 kN load cell with an accuracy of 0.04 kN. The actuators were driven by hydraulics and were servo-controlled by an Instron 8800 dual digital controller. In this apparatus, shear loads can be applied by load control or displacement control, and under either cyclic or monotonic loading conditions. CNS conditions are imposed by putting the vertical actuator in load control and imitating a spring with stiffness K, using a feedback mechanism (see Fig. 16).

The shear load for the tests described in this research study was delivered using monotonic single ramp waveforms and the horizontal actuator was controlled by displacement. Two internal and three exterior linear variable displacement transducers (LVDTs) were used to measure displacements (Fig. 17). Internal LVDTs were installed within the actuators and used to measure actuator displacement. To measure

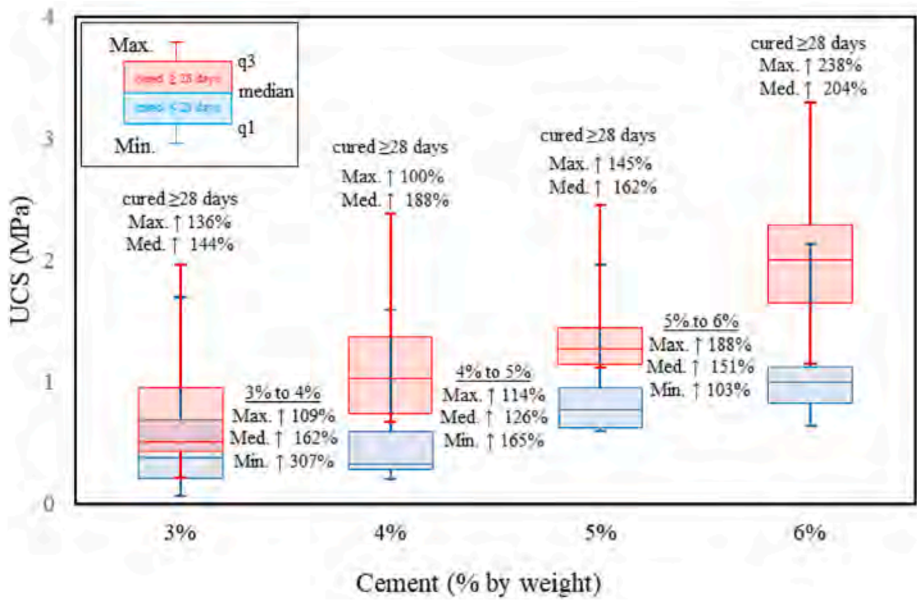

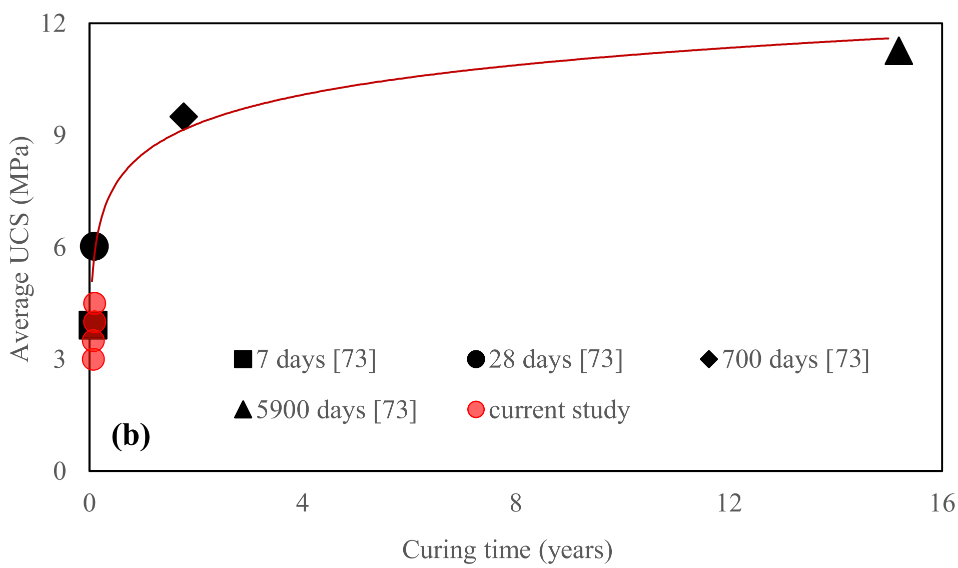

Fig. 14. a) Database of relationships between cement content and curing time, b) average UCS versus curing time for CRF samples from TRJV mine [9,18,73] and current study.

vertical displacement (e.g., dilation), two external LVDTs were employed. Each was installed on the top of shear box and measured the distance to a reference plate located on the bottom of shear box. Shear displacement was measured using an external LVDT. The magnetic base of this LVDT was attached to the frame of the shear apparatus, and the tip is put against the end of the shear box. Roller bearings were utilised by the vertical piston that applied normal stress to the sample to restrict rotation of the top and bottom sections of the shear box and to reduce friction losses.

The shear box itself is constructed from two steel plate sections that hold the sample with size of 600 mm length, 200 mm height, and 160 mm depth. Steel plates on the sides, top, bottom, and rear of the shear box hold the sample in place, while 20 mm thick perspex constrains the front. The perspex front is supported with steel to minimise any outward deflection caused by sample dilation during shearing. The CNS shear equipment is connected directly to the shear box. External LVDTs and reference plates were installed after the separator strips connecting the top and lower parts of the shear box. Under CNS settings, the upper part of the shear box was permitted to dilate. The bottom half of the shear box can displace up to 60 mm allowing measurements of the pre-peak and post-peak behaviour.

At the start of each test, the sample was subjected to an initial (vertical) normal stress. The normal stress increased or reduced depending on the amount of dilation and the defined normal stiffness after the test commenced. The sample was sheared by lateral displacement of the bottom of the shear box and vertical dilation of the top of the sample against a specified stiffness. A shear rate of 0.5 mm/min was applied. Apart from boundary conditions, Bahaaddini [90] found that the size of the gap zone between the upper and lower shear boxes has an influence on the shear mechanism. During the testing, 40 mm dilation of the sample was common which is directly related to the particle size of the samples.

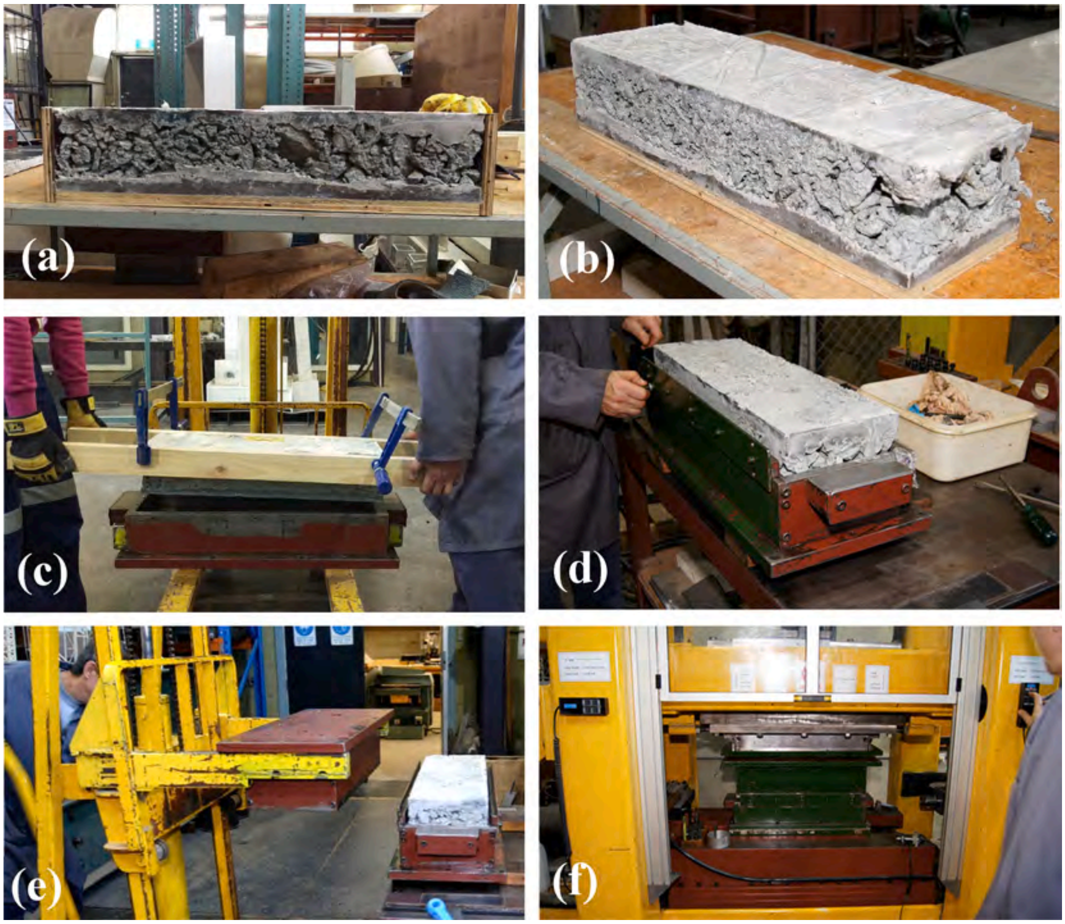

Fig. 15. a) b) Direct Shear cured sample, c) d) e) sample seating, and f) test set-up.

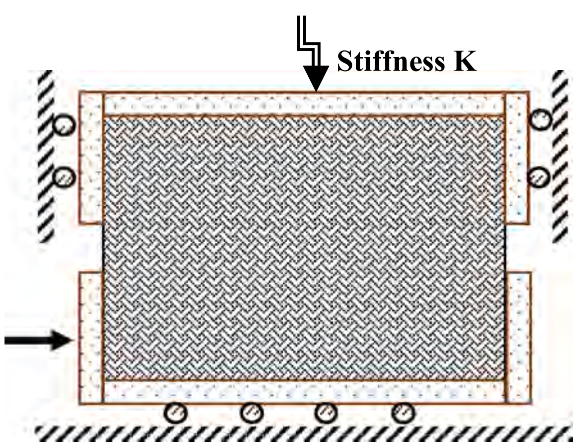

Fig. 16. Schematic for NCS boundary condition [82–84].

5.3. Test results

Direct shear test results were successfully conducted for a total of eight samples, seven samples of CRF: CRF and one sample of CRF: Sidewall. The seven CRF: CRF samples were completed for normal stresses of 50, 100, 200 kPa. The CRF: Sidewall test was completed with 100 kPa normal stress. An example of sample dilation during shearing is presented in Fig. 17.

An increasing shear strength is observed for the CRF: CRF samples as the normal stress is increased. In each case, the first yield can be attributed to locally degrading cement bonds and matrix deformation, while the rise in strength to the second yield (and subsequent failure) is considered to be induced by particle interlocking and dislocation. This is described as strain-hardening behaviour that is typical of granular material [91]. Similar tendencies were detected in in-situ shear experiments conducted by Coli et al. [92]. A difference is observed between CRF: CRF and CRF: Sidewall direct shear test results. Example results for each of the sample types are presented in Fig. 19 along with records of the sheared surface conditions at the completion of the tests.

In both instances, a surface fracture profile occurs that passes through the cementitious bonds following the contour of the rock aggregate particles. However, the surface profiles of each CRF samples are different due to the heterogeneous stress distribution within the mass that is frequent in direct shear experiments and determined by the particle contacts [78]. The lower strength of the CRF: CRF sample suggests that a change in failure mechanism is observed between the contact surfaces. If sliding was the pre-peak behaviour, it is expected that changes in the CRF contact surface would have no effect on the pre-peak process. Thus, there is a possibility that a shear failure mechanism (and hence peak strength) may also be influenced by rotational behaviour of the particles. In the case of CRF: Sidewall contact, strain-hardening behaviour is observed at the peak strength of the CRF: CRF samples. An interpretation of the CRF: CRF, and CRF: Sidewall direct shear results are presented in Fig. 20. The results of the direct shear testing have been interpreted to provide both peak and residual effective strength parameters cohesion (c) and friction angle (ϕ).

The large-scale testing has shown that the direct shear responses between the CRF and excavation sidewalls are significantly higher (~150%) than CRF on CRF contacts. A linear Mohr-Coulomb interpretation of the shear strength parameters has been made for minor principal stresses up to 0.2 MPa within the fill-mass. For a 6% CRF, peak

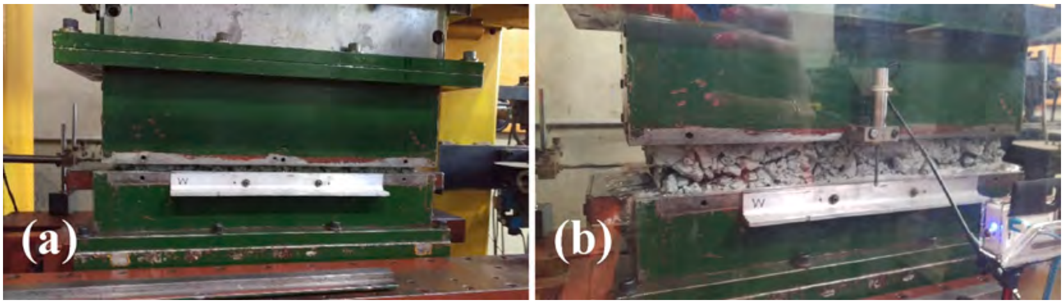

Fig. 17. a) Direct shear sample set-up b) dilation after testing.

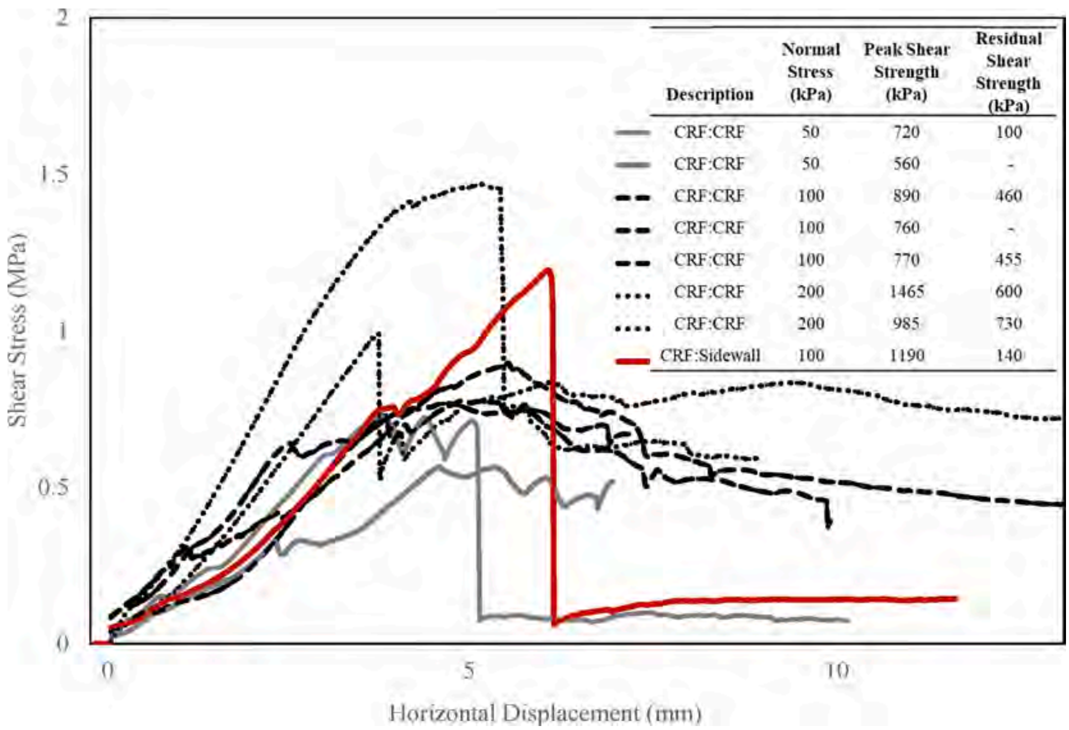

Fig. 18. Direct shear stress–strain results.

cohesion and friction of 0.079 MPa and 40° can be used. Residual values of 0.036 MPa and 28° have been determined. This result is particularly important for exposure stability studies and provides material properties for the CRF: Sidewall contact interface for numerical exposure analysis models.

6. Three-Point bending tensile testing

Previous research studies demonstrated the significance of CRF tensile strength due to blast-induced vibrations in the topmost region of an exposed CRF stope [21]. Tensile test results are also important for overhand exposures since they represent the most common in-situ failure mode. Furthermore, when extraction occurs adjacent to CRF pillars, the tensile property of CRF become increasingly critical. However, few tensile laboratory tests have been completed on CRF [27,93] and, as such, similar to rock, a tensile to compressive strength ratio of 10% is typically assumed [1]. The drawback of not measuring tensile strength of CRF directly, is that, in most in-situ cases, the tensile capacity is the critical limiting design case [94]. Mitchell and Wong [95] conducted a series of tensile strength tests on cemented tailings sands using both the three-point bending (3 PB) method and direct tension testing. Tensile strengths from both tests gave similar results; the average tensile strength was found to be 12% of the UCS. Through these experiments on stabilised backfill material, it was found that three-point bending tests provided a reliable estimation of the tensile strength [96], and as such has been applied herein.

6.1. Sample preparation

A number of large-scale three-point bending tests have been completed on 6% (wt.) CRF samples have been cured for 28-days. The testing procedure and sample size are consistent with the standard ASTM procedures to satisfy simple beam theory [97]. Samples were prepared and cured in custom-made moulds with dimensions 300 mm × 300 mm × 1200 mm. A thin concrete 'cap' was placed in the centre of the sample at the loading point to ensure that point loading of the sample did not occur. The size and weight of the samples make these tests especially challenging within the laboratory. Fig. 21 provides an overview of a three-point bending sample being prepared for testing. The sample side wall moulds are removed after seating the sample. Once in place, the base of the mould is also removed prior to loading.

6.2. Testing apparatus

A 600-kip, manual-hydraulic driven, stiff-frame testing machine was used to test the 300 mm × 300 mm × 1200 mm cubical samples. An

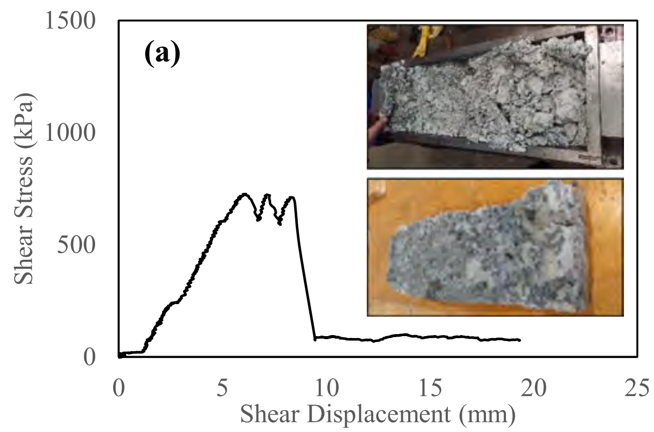

Fig. 19. Typical direct shear sample response and failure surface (a) CRF: CRF (b) CRF: Sidewall.

Amsler compression load frame with an axial load capacity of up to ± 5000kN was used for the static three-point bending testing of the large-scale samples. The tests were carried out with the aid of computer-controlled loading at a rate of 0.05 mm/min. The load at failure was translated into a tensile strength through the relationship presented in Equation. (2).

$$\frac{3}{2}\frac{FL}{wt^2} \tag{2}$$

where F is the applied force at failure (N), L is the length of the sample (m), w is the width of the sample (m) and t is the thickness of the sample (m).

6.3. Test results

The load–displacement results of four 3 PB tests are presented in Fig. 22. For each sample the particle size distribution is observably different. Sample (c) has the greatest average particle size, sample (a) has the smallest average particle size.

The pre-peak strength-displacement trend is similar for all tests with the stress–strain curves exhibiting a non-linear concave upwards section at the commencement of loading. This is due to the porous texture of the specimens and closure of voids. This early non-linearity becomes more apparent in specimens with a higher particle size distribution (e.g., coarser average particle size – Fig. 22 sample c). The majority of CRF samples deformed between 3 and 4 mm. The observed tensile strength for the 6% (wt.) was approximately 200–370 kPa which is approximately 20% of the measured UCS in this study for the same particle size and cement content. This finding has also been observed at other mine sites (Fig. 23).

The test results indicate that the “12% of the UCS” [95] rule-of-thumb for cemented tailings sand may be conservative when applied to the tensile strength of CRF. This result is particularly significant since, in most exposure stability analyses tension has been the limiting factor for design of CRF strength (based on UCS) [1]. It is therefore proposed that the cement content of CRF mixtures may be significantly reduced when the results of stability analyses can accurately predict the stress-path and material response. In addition, it has to be accepted that the

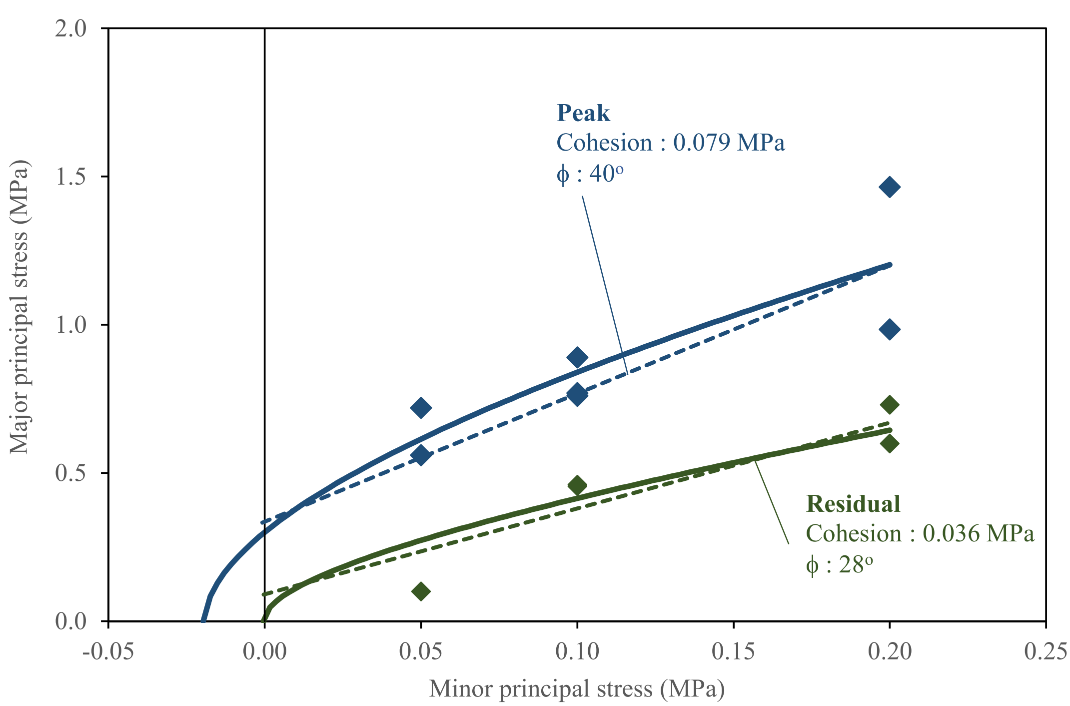

Fig. 20. Fitted peak and residual effective strength parameters for 6% CRF at low (0.2 MPa) confinement.

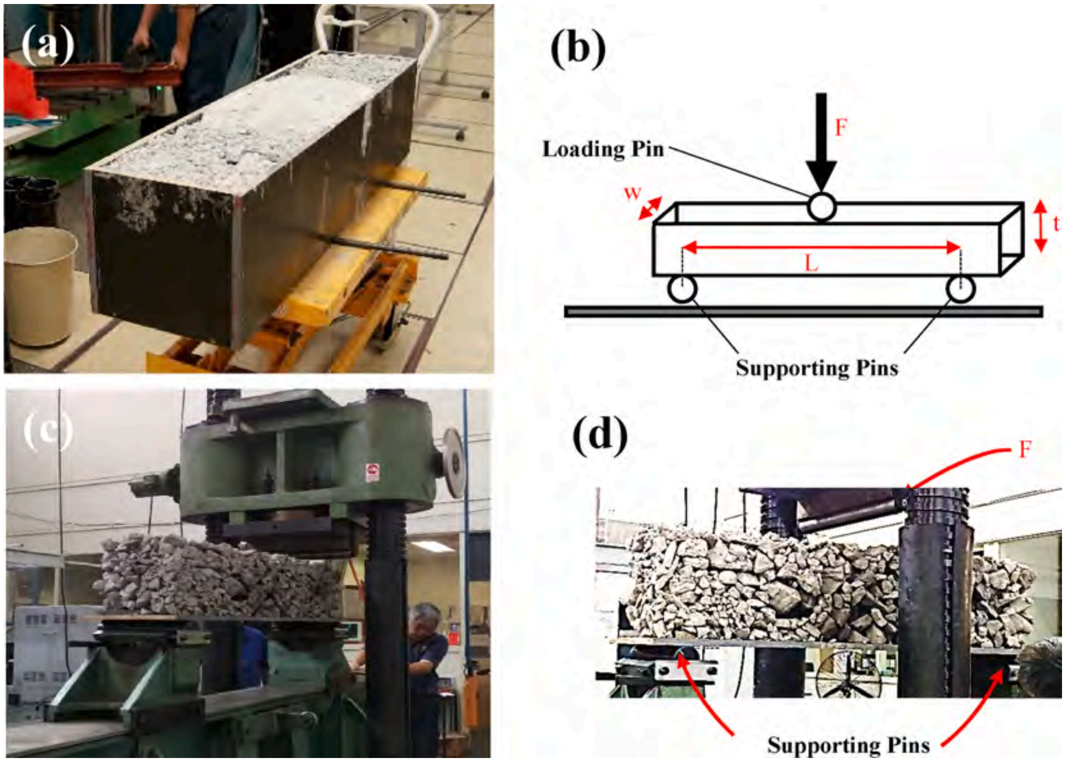

Fig. 21. a) Three-point bending sample, b) schematic test set-up, c) sample seating, and d) annotated testing set-up.

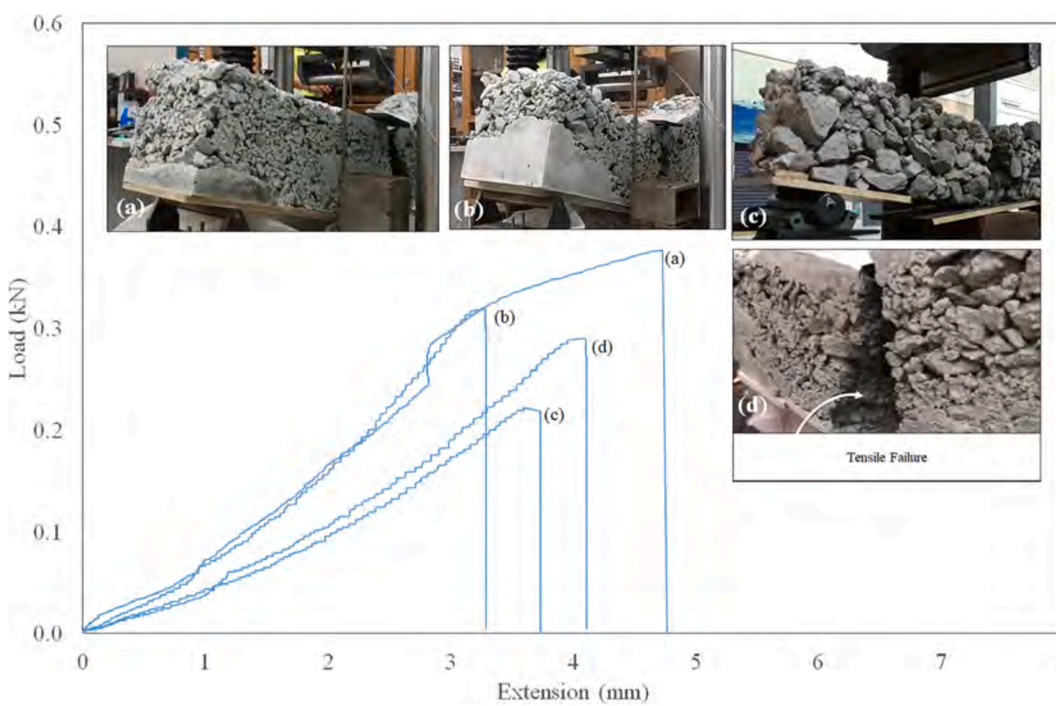

Fig. 22. Three-Point Bending test results, for CRF samples with 6% cement.

PSD is extremely important to analyse the tensile test results, and in this case, may be more critical than cement content to determine the material response. With the same cement content, a higher tensile strength obtained for smaller average particle size (Fig. 22 sample (a)), this behaviour is also observed in UCS test results (Figs. 12, 13).

Fig. 23 also compares the current three-point bending test results to splitting tensile strength tests for various mine sites. It is true that the average tensile strength of CRF samples can be related to their average compressive strength, as illustrated by the dotted line in Fig. 23. However, it is observed that most of the three-point bending test results are more than 10% of the average UCS. Combined with the current 3 PB test results, splitting tensile strength (STS) test findings for CRF samples from the TRJV, CHUG, and Stillwater mines demonstrate that the average tensile strength of CRF is at least 15%-20% of its UCS. Despite

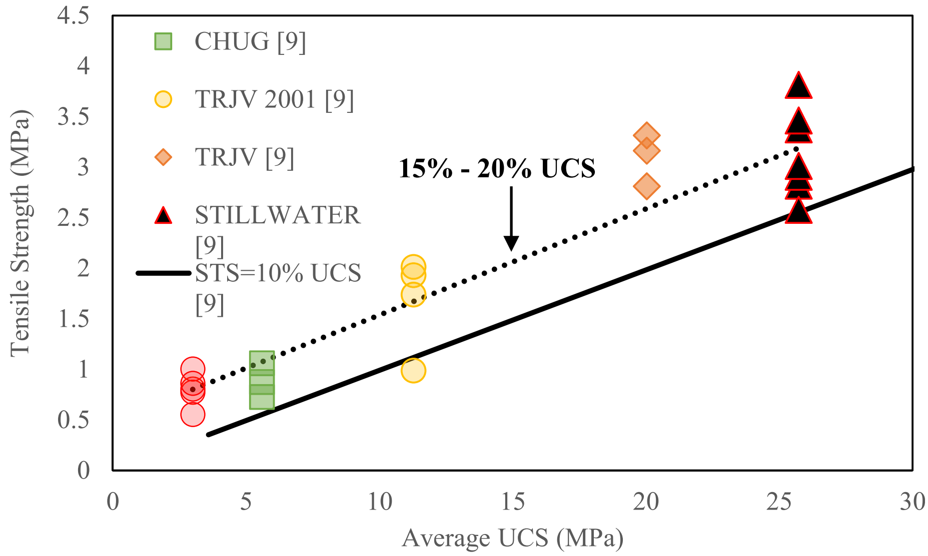

Fig. 23. Splitting tensile strength (STS) against average UCS for CRF samples from TRJV, CHUG, and Stillwater mine sites [9], and three-point bending tensile test results in the current study.

the variance in mix design, particle size distribution, and tensile testing methodology, all of the experimental data agree and show a similar trend that 10% of the UCS is a conservative estimate of the tensile strength of CRF structures at mines. This may be resulting in the over-design of these structures causing unnecessary cost.

7. Conclusion and future works

A rigorous experimental testing program for CRF material must include the characterization of all three failure modes; crushing, shearing and tension at large sample sizes. To characterize these failure modes, UCS, direct shear and three-point bending tests are all required to be completed to replicate these specific stress paths.

The results of large-scale UCS, tension and direct shear tests are provided herein to provide geomechanical data for CRF for exposure stability analysis. The results of the large-scale testing show that an increased cement content increases the UCS strength, stiffness, and post-peak brittleness of the CRF mixture. The full stress–strain curves show that as cement content increases, so does the post-peak brittleness, transitioning from characteristically ductile responses at 3% cement to perfectly brittle at 8% cement content.

It must be acknowledged that conducting physical tests on large-scale CRF samples with constant normal stiffness (CNS) boundary conditions is quite challenging [78]. However, herein we prepared and tested large-scale CRF samples under CNS boundary conditions. Results measure the peak and residual shear properties of CRF at cohesion 0.079 MPa, $\phi = 40^{\circ}$ and cohesion 0.036 MPa, $\phi = 28^{\circ}$, respectively. Testing has shown that the direct shear responses between the CRF and excavation sidewalls are significantly higher (~150%) than CRF on CRF contacts. This result is particularly important for exposure stability studies.

In addition, the large-scale testing has shown that tensile strength responses are significantly higher, at up to 20% of the UCS strength than previously estimated. This result is particularly significant since, in most exposure stability analyses [1] tension has been the limiting design factors. It is therefore proposed that the cement content of CRF mixtures may be significantly reduced for specific stress paths (exposure histories).

7.1. Future works

Due to the size restrictions of most monitoring equipment, quantifying sample deformations using classic strain monitoring techniques such as LVDTs is often difficult. Furthermore, misalignment is a common source of uncertainty during deformation measurements. Therefore, a more flexible measuring instrument based on digital image correlation (DIC), is recommended. Digital image correlation (DIC) can be used to determine damage (particle bond breakage) within a CRF sample during failure within the laboratory and correlated with in-situ observations of stability.

A vibrating table [98] or a vibrating compaction hammer [99] may be used in the preparation of CRF samples to develop more consistent compaction or density values for CRF. However, in in-situ conditions, there is little control on these parameters during placement.

The maximum particle size of waste rock aggregates after screening is usually bigger than the screen size. Due to the fact that these devices only screen in one dimension, elongated and tabular aggregates with diameters larger than the bar spacing can pass the screen. If the CRF aggregate is screened more thoroughly using perpendicular bars, more consistent test results may be achieved through the consideration of particle shape.

The inclusion of additives or stabilisers that may be classified as ‘waste’ at a mining operation (e.g., tyres) could also be considered to increase the flexural and energy absorbing capacity of the backfill material while also minimising landfill and waste dump requirements.

The shear response of CRF may be further investigated using a combined direct shear and triaxial approach [25,45,46]. A comprehensive understanding regarding the advantages and disadvantages each of direct shear and triaxial testing can be found in references [100-103]. It is recommended that further shear testing should focus on internal CRF particle deformation, interlocking and dilation and/or the response of CRF when mobilised along the sidewall rock contacts. Internal interactions between CRF particles with high variability in size has been shown to be characterised most efficiently through triaxial testing [25,45,46]. However, limitations associated with the size of the triaxial cell required (400 mm dia.) remains a challenge [45].

Declaration of Competing Interest

The authors declare that they have no known competing financial interests or personal relationships that could have appeared to influence the work reported in this paper.

Acknowledgement

The authors would like to thank Monash University, for providing some of the laboratory resources to conduct this research study. The authors were previously employed there.

References

[1] D.P. Sainsbury, B. Sainsbury, Design and implementation of cemented rockfill at the ballarat gold project. mine fill proceeding, Int Symp. Min. with Backfill 11 (2014) 1–12.
[2] P.N. Farsangi, Improving cemented rockfill design in open stoping, PhD thesis, McGill University, 1996.
[3] M. Kockler, Design of cemented rockfill spans for longhole stoping at the Rain Mine, University of Idaho, PhD thesis (2007).
[4] B. Van Gool, Effects of blasting on the stability of paste fill stopes at Cannington Mine, PhD thesis, James Cook University (2007).
[5] D. Finn, M. Dorricott, Cemented rock fill for extraction of high-grade crown pillars at crusader gold mine, Australasia Inst. Min. Metall. Publ. Ser. 5 (2002) 177–180.
[6] B. Sainsbury, D. Sainsbury, J. Western, P.E. Petrie, V. Mutton, Pillar recovery adjacent to stabilised rockfill at the ballarat gold project, AusRock Third Australas Gr. Control Min. Conf. (2014) 77–86.
[7] G. Lu, X. Yang, S. Qi, G. Fan, J. Zhou, Coupled chemo-hydro-mechanical effects in one-dimensional accretion of cemented mine fills, Eng. Geol 267 (2020), 105495.
[8] J. Wu, M. Feng, X. Ni, X. Mao, Z. Chen, G. Han, Aggregate gradation effects on dilatancy behavior and acoustic characteristic of cemented rockfill, Ultrasonics 92 (2019) 79–92.
[9] S.N. Warren M.J. Raffaldi K.K. Dehn J.B. Seymour Estimating the strength and mechanical properties of cemented rockfill for underhand cut-and-fill mines 2018 Washington, USA 18 873.
[10] Y. Li, S. Zhang, R. Wang, F. Dang, Potential use of waste tire rubber as aggregate in cement concrete-a comprehensive review, Constr. Build. Mater. 225 (2019) 1183–1201.
[11] A.J. Choobbasti, A. Vafaei, S.S. Kutanaei, Static and cyclic triaxial behaviour of cemented sand with nanosilica, J. Mater. Civ. Eng. 30 (10) (2018) 04018269.
[12] A.J. Choobbasti, M.A. Samakoosh, S.S. Kutanaei, Mechanical properties soil stabilized with nano calcium carbonate and reinforced with carpet waste fibers, Constr. Build. Mater. 211 (2019) 1094–1104.
[13] A.J. Choobbasti, S.S. Kutanaei, Microstructure characteristics of cement-stabilized sandy soil using nanosilica, J. Rock Mech. Geotech. Eng. 19 (2017) 981–988.
[14] A.J. Choobbasti, A. Vafaei, S.S. Kutanaei, Mechanical properties of sandy soil improved with cement and nanosilica, Open Eng 5 (2015) 111–116.
[15] M. Ghadakpour, A.J. Choobbasti, S.S. Kutanaei, Investigation of the deformability properties of fiber reinforced cemented sand, J. Adhes. Sci Technol. 33 (17) (2019) 1913–1938.
[16] M. Cordova, H. Saw, E. Villaescusa, Laboratory testing of cemented rock fill for open stope support. Seventh International Conference & Exhibition on Mass Mining Sydney, 2016.
[17] H. Jiang, M. Fall, Y. Li, J. Han, An experimental study on compressive behaviour of cemented rockfill, Constr. Build. Mater. 213 (2019) 10–19.
[18] J.B. Seymour, L.A. Martin, M.J. Raffaldi, S.N. Warren, L.A. Sandbak, Long-Term stability of a 13.7 × 30.5-m (45 × 100-ft) undercut span beneath cemented rockfill at the Turquoise Ridge Mine, Nevada, Rock Mech. Rock Eng. 52 (12) (2019) 4907–4923.
[19] D.R. Tesarik, J.B. Seymour, T.R. Yanske, Post-failure behavior of two mine pillars confined with backfill, Int. J. Rock Mech. Min. Sci. 221–232 (2003).
[20] D. Marschi, C. Chan, H. Seed, Evaluation of properties of rockfill materials, ASCE J. Soil Mech. Found. 98 (1) (1972) 95–114.
[21] M.Z. Emad, H.S. Mitri, J.G. Henning, Effect of blast vibrations on the stability of cemented rockfill, Int. J. Min. Reclam. Env. 26 (3) (2012) 233–243.
[22] M.Z. Emad, H. Mitri, C. Kelly, In-situ blast vibration monitoring in cemented rockfill stope–a case study, Int. J. Mining, Reclam. Environ. 31 (2) (2017) 119–136.
[23] J. Zhang, B. Li, N. Zhou, Q. Zhang, Application of solid backfilling to reduce hard-roof caving and longwall coal face burst potential, Int. J. Rock Mech. Min. Sci. 88 (2016) 197–205.
[24] B.A. Lingga, Investigation of cemented rockfill properties used at a Canadian Diamond Mine, Universit of Alberta, MSc thesis (2018).
[25] B.A. Lingga, D.B. Apel, Shear properties of cemented rockfills, J. Rock. Mech. Geotech. Eng. 10 (4) (2018) 635–644.
[26] P.B. Hughes, Design guidelines: underhand cut and fill cemented paste backfill sill beams, PhD thesis, University of British Columbia, 2014.
[27] R.J. Mitchell, Sill mat evaluation using centrifuge models, Min. Sci. Technol. 13 (3) (1991) 301–313.
[28] K. Terzaghi, Theoretical soil mechanics, Wiley, New York, 1943.
[29] R. Pakalnis, C. Caceres, K. Clapp, M. Morin, T. Brady, T. Williams, W. Blake, M. MacLaughlin, Design spans – underhand cut and fill mining 9 (2005) 1–9.
[30] K. Terzaghi, R.B. Peck, G. Mesri, Soil mechanics in engineering practice, Wiley and Sons, New York, 1996, pp. 1–549.
[31] S.A. Ghoreishi-Madiseh, F. Hassani, F. Abbasy, Numerical and experimental study of geothermal heat extraction from backfilled mine stopes, Appl. Therm. Eng. 90 (5) (2015) 1119–1130.
[32] W. Wu, W. Xu, J. Zuo, Effect of inclined interface angle on shear strength and deformation response of cemented paste backfill-rock under triaxial compression, Constr. Build. Mater. 279 (2021), 122478.
[33] Q. Liu, D. Liu, Y. Tian, X. Liu, Numerical simulation of stress-strain behaviour of cemented paste backfill in triaxial compression, Eng. Geol. 231 (2017) 165–175.
[34] M. Sepehri, D. Apel, R. Hall, Prediction of mining-induced surface subsidence and ground movements at a Canadian diamond mine using an elastoplastic finite element model, Int. J. Rock Mech. Min. Sci. 100 (2017) 73–82.
[35] B.A. Lingga, D.B. Apel, M. Sepehri, Y. Pu, Assessment of digital image correlation method in determining large scale cemented rockfill strains, Int. J. Min. Sci. Technol. 29 (5) (2019) 771–776.
[36] J. Wu, M. Feng, X. Mao, J. Xu, W. Zhang, X. Ni, G. Han, Particle size distribution of aggregate effects on mechanical and structural properties of cemented rockfill: Experiments and modeling, Constr. Build. Mater. 193 (2018) 295–311.
[37] L. Li, M. Aubertin, A modified solution to assess the required strength of exposed backfill in mine stopes, Can. Geotech. J. 49 (8) (2012) 994–1002.
[38] H. Saw, S. Prentice, E. Villaescusa, Characterisation of cemented rock fill materials for the Cosmos nickel mine. Western Australia, in International Conference on Advances in Construction Materials through Science and Engineering, 2011.
[39] R.J. Mitchell J.J. Roettger Analysis and modelling of sill pillars, Innovations in mining backfill technology 1989 Balkema, Rotterdam 53 62.
[40] D. Kumar, U.K. Singh, G.S.P. Singh, U. Kumar Singh, G., Shankar Prasad Singh, Laboratory characterization of cemented rock fill for underhand cut and fill method of mining, J. Inst. Eng. Ser. D 97 (2) (2016) 193–203.
[41] M. Fall, T. Belem, S. Samb, M. Benzaazoua, Experimental characterization of the stress-strain behaviour of cemented paste backfill in compression, J. Mater. Sci. 42 (11) (2007) 3914–3922.
[42] B.K. Shrestha, D.D. Tannant, S. Proskin, J.R.S. Greer, Properties of cemented rockfill used in an open pit mine, GeoEdmonton 08 (2008) 609–616.
[43] N. Barton, V. Choubey, The shear strength of rock joints in theory and practice, Rock. Mech. Rock. Eng. 10 (1977) 1–54.
[44] J. Wu, H. Jing, Q. Yin, B. Meng, G. Han, Strength and ultrasonic properties of cemented waste rock backfill considering confining pressure, dosage and particle size effects, Constr. Build. Mater. 242 (2020), 118132.
[45] A.F. Sevi, L. Ge, W.A. Take, A large-scale triaxial apparatus for prototype railroad ballast testing, Geotech. Test. J. 32 (4) (2009) 297–304.
[46] E. Fortunato, A. Pinelo, M.M. Fernandes, Characterization of the fouled ballast layer in the substructure of a 19^{th} century railway track under renewal, Soils Found. 50 (1) (2010) 55–62.
[47] A. Talbot, F. Richart, The strength of concrete, its relation to the cement aggregates and water, University of Illinois, Engineering Experiment Station. Bulletin. 137 (1923).
[48] D. Stone, The optimization of mix designs for cemented rockfill, Minefill 93 (1993).
[49] M. Li, J. Zhang, N. Zhou, Y. Huang, Effect of Particle Size on the Energy Evolution of Crushed Waste Rock in Coal Mines, Rock Mech. Rock Eng. 50 (5) (2017) 1347–1354.
[50] B. Salvoldi, B. van der Spuy, S. Wilson, Optimisation of cemented aggregate backfill at New Luika Gold Mine, Proc. 22nd Int. Conf. Paste, Thick. Filtered Tailings (2019) 437–450.
[51] ASTM Standard C172/C172M-17, Standard Practice for Sampling Freshly Mixed Concrete. West Conshohocken, PA (2017).
[52] A.M. Neville, Properties of Concrete, 4th ed., Pearson Prentice Hall, Harlow, England, 2009.
[53] Bureau of Reclamation. Concrete Manual. U.S. Department of the Interior, Water and Power Resources Service, 8th ed. Washington DC: U.S. Government Printing Office, (1981).
[54] N. Marachi, Strength and deformation characteristics of rockfill materials, PhD thesis, University of California, Berkeley, 1969.
[55] F. Emha, Shear strength of Bremanger sandstone rockfill at low stress, Delft University of Technology, MSc thesis (2011).
[56] ASTM Standard C192/C192M-13a, Standard Practice for Making and Curing Concrete Test Specimens in the Lab. Annual Book of ASTM Standards, West Conshohocken, PA, (2013).
[57] J. Wu, M. Feng, Z. Chen, X. Mao, G. Han, Y. Wang, Particle size distribution effects on the strength characteristic of cemented paste backfill, Minerals. 8 (8) (2018) 1–21.
[58] C. Wang, E. Villaescusa, Influence of water salinity on the properties of cemented tailings backfill, Inst. Min. Metall. Trans. Sect. A Min. Technol. 110 (2001).
[59] D. Stone, Factors that affect cemented rockfill quality in Nevada mines, CIM Bull. 100 (1103) (2007) 1–24.
[60] M.E. Pierce, Laboratory and numerical analysis of the strength and deformation behaviour of paste backfill, MSc thesis, Queens University, 1997.
[61] T. Belem, M. Benzaazoua, Design and application of underground mine paste backfill technology, Geotech. Geol. Eng. 26 (2) (2008) 147–174.
[62] C.D. Lawrence, The influence of binder type on sulfate resistance, Cem Concr Res 22 (1992) 1047–1058.

[63] M. Benzaazoua, J. Ouellet, S. Servant, P. Newman, R. Verburg, Cementitious backfill with high sulfur content: Physical, chemical and mineralogical characterization, Cem Concr Res 29 (1999) 719–725.
[64] ASTM C143-90. Standard test method for slump of hydraulic cement concrete. Annual book of ASTM Standards, 4 (1998) United States.
[65] G. Swan, A new approach to cemented backfill design, CIM Bulletin 78 (884) (1985) 53–58.
[66] ASTM C33. Standard Specification for Concrete Aggregates. (2003) 1-11.
[67] C.E. Fairhurst, J.A. Hudson, Draft ISRM suggested method for the complete stress–strain curve for intact rock in uniaxial compression, Int. J. Rock. Mech. Min. Sci. 36 (1999) 279–289.
[68] ASTM C617/C617M – 12. Standard Practice for Capping Cylindrical Concrete Specimens. (2012) 1–6.
[69] S. Van Der Merwe, Backfill management plant, Cosmos nickel operations, unpublished internal report, Xstrata Nickel Australia.
[70] B.A. Sainsbury, A,, model for cave propagation and subsidence assessment in jointed rock masses, PhD thesis, University of New South Wales, 2012.
[71] E.T. Brown, Rock characterization, testing and monitoring – ISRM suggested methods, Pergamon, Oxford, 1981, pp. 171–183.
[72] D. R. Tesarik, J.B. Seymour, F.M. Jones, Determination of in-situ deformation modulus for cemented rockfill. In Proceeding of 10th Congress of International Society for Rock Mechanics, Johannesburg, South Africa, 8-12 September 2003, eds. M. Handley and D. Stacey, 1209-1220, Johannesburg: SAIMM.
[73] J.B. Seymour, M.J. Raffaldi, S.N. Warren, L.A. Martin, Long term stability of a large undercut span beneath cemented rockfill at the Turquoise Ridge Mine, in: R. Schultz (Ed.), In Proceeding of the 52nd U.S. Rock Mechanics/ Geomechanics Symposium, 2018, pp. 1–16.
[74] E. Hoek, E.T. Brown, Underground excavations in rock, The Institution for Mining and Metallurgy, Taylor and Francis, London, 1980.
[75] S.H. Kosmatka, W.C. Panarese, Design and control of concrete mixtures, 13th ed., Portland Cement Association, Skokie, Illinois, 1988.
[76] N.J.F. Koupouli, T. Belem, P. Rivard, H. Effenguet, Direct shear tests on cemented paste backfill–rock wall and cemented paste backfill–backfill interfaces, J. Rock Mech. Geotech. Eng. 8 (4) (2016) 472–479.
[77] N. Koupouli, T. Belem, P. Rivard, Shear strength between cemented paste backfill and natural rock surface replicas, in Underground Mining Technology (2017) 375-385.
[78] J. Shang, Z. Zhao, S. Ma, On the shear failure of incipient rock discontinuities under CNL and CNS boundary conditions: Insights from DEM modelling, Eng. Geol. 234 (2018) 153–166.
[79] M. Fahey, M. Helinski, A. Fourie, "Some aspects of the mechanics of arching in backfilled stopes, Can. Geotech. J. 46 (11) (2009) 1322–1336.
[80] N. Barton, The shear strength of rock and rock joints, Int. J. Rock. Mech. Min. Sci. Geomech. Abstr. 13 (9) (1976) 255–279.
[81] J. Zhao, Joint surface matching and shear strength part B: JRC-JMC shear strength criterion, Int. J. Rock. Mech. Min. Sci. 34 (2) (1997) 179–185.
[82] H. Pearce, Shear behaviour of rock joints, Monash University, PhD thesis, Melbourne, (2001).
[83] J. Szymakowski, Direct shear testing of jointed soft rock masses, PhD thesis, Monash University, 2003.
[84] J. Szymakowski, Shear testing of soft rock masses, Geotech. Test. J. 30 (2) (2006) 133–140.
[85] A. Shrivastava, K. Rao, Development of a large-scale direct shear testing machine for unfilled and infilled rock joints under constant normal stiffness conditions, Geotechnical Testing Journal. 36 (5) (2013) 670–679.
[86] S. Poturovic, W. Schubert, M. Blümel, Comparison of constant normal load (CNL) and constant normal stiffness (CNS) direct shear tests, ISRM-EUROCK, Salzburg, Austria, October, 2015.
[87] K. Thiel, L. Zabuski, Failure phenomena in large-scale direct shear test. The 2nd North American Rock Mechanics Symposium, Montreal, Quebec, Canada, June (1996).
[88] A.J. Afridi, S. Kwon, J.W. Wilson, Investigation of rock failure in a direct shear machine, Transactions of the Institution of Mining and Metallurgy, Section A: Mining Technology 110 (2001) 158–162.
[89] N. Barton, V. Choubey, The shear strength of rock joints in theory and practice, Rock Mechanics. 10 (1) (1977) 1–54.
[90] M. Bahaaddini, Effect of boundary condition on the shear behaviour of rock joints in the direct shear test, Rock. Mech. Rock Eng. 50 (2017) 1141–1155.
[91] B. Sainsbury, Consideration of the volumetric changes that accompany rock mass failure, Rock. Mech. Rock. Eng. 52 (2019) 277–281.
[92] N. Coli, P. Berry, D. Boldini, In-situ non-conventional shear tests for the mechanical characterisation of a bimrock, Int. J. Rock. Mech. Min. Sci. 48 (1) (2011) 95–102.
[93] M. Dundu, X. Gao, Construction materials and structure, IOS Press BV, Netherlands, 2014.
[94] I. Vennes, Determination of cemented rockfill strength with large scale UCS tests under in-situ conditions, MSc thesis, McGill University, 2014.
[95] R.J. Mitchell, B.C. Wong, Behaviour of cemented tailings sands, Can. Geotech. J. 19 (3) (1982) 289–295.
[96] ASTM C78-b, Standard Test Method for Flexural Strength of Concrete (Using Simple Beam with Third-Point Loading), Am. Soc. Test. Mater. West Conshohocken, PA, USA. (2015) 1–4.
[97] L. Euler, The rational mechanics of flexible or elastic bodies: Introduction to, Vol. X and XI, Birkhauser (1960) 1638–1788.
[98] ASTM Standard C1176/C1176M-13, Standard Practice for Making Roller-Compacted Concrete in Cylinder Molds Using a Vibrating Table. West Conshohocken, PA (2013).
[99] ASTM Standard C1435/C1435M-14, Standard Practice for Molding Roller-Compacted Concrete in Cylinder Molds Using a Vibrating Hammer. West Conshohocken, PA: (2014).
[100] E.Z. Lajtai, Shear strength of weakness planes in rock, Int. J. Rock. Mech. Min. Sci. 6 (1969) 499–515.
[101] F. Gong, S. Luo, G. Lin, X. Li, Evaluation of shear strength parameters of rocks by preset angle shear, direct shear and triaxial compression tests, Rock. Mech. Rock. Eng. 53 (2020) 2505–2519.
[102] N.R. Malidarreh, I. Shooshpasha, S.M. Mirhosseini, M. Dehestani, Effects of reinforcement on mechanical behaviour of cement treated sand using direct shear and triaxial tests, Int. J. Geotech. Eng. 12 (5) (2018) 491–499.
[103] R.S. Rosso, A comparison of joint stiffness measurements in direct shear, triaxial compression, and In Situ, Int. J. Rock. Mech. Min. Sci. Geomech. Abstra. 13 (6) (1976) 167–172.